Strengthening lightweight long-span timber floors: A study on vibration performance and human perception

Farid Piran [a], Hassan Karampour [a,*] , Hong Guan [a] , Chandan Kumar [b], Huaizhong Li [a], Guido Carim Junior [a]

[a] *School of Engineering and Built Environment, Griffith University, Gold Coast Campus, QLD 4222, Australia*
[b] *Agri-Science Queensland, Department of Primary Industries, Salisbury, Brisbane, QLD 4107, Australia*

ARTICLE INFO

ABSTRACT

Floor vibration is a common serviceability issue in low-rise commercial buildings across Australia with lightweight long-span timber floors (LSTFs). In the absence of validated dynamic properties, calibrated numerical models, analytical reliable methods for predicting vibration responses and sufficient studies on human perception of vibration in LSTFs, developing an efficient design becomes challenging. This study aims to provide insights into these unknowns for a simply supported 8-meter LSTF comprised of steel-wood timber truss (SWTT) joists with a particleboard slab. The research experimentally measures static deflection, natural frequencies, and mode shapes of both the SWTT and the LSTF, and uses these results to validate the numerical models. Responses to footfall excitations of the LSTF, both with and without strengthening using strongbacks, are measured through comprehensive walking tests and surveys of participants. The experimental measurements and survey results are compared with predictions from existing international guidelines recommended for designing floors to resist footfall-induced vibrations. It is demonstrated that the inclusion of strongbacks is an effective method for mitigating excessive vibrations, both from the participants' perspective and in terms of standard compliance. The correlations between participant survey results obtained through virtual reality (VR) technology and the comfort criteria recommended in international guidelines are highlighted in the discussion.

1. Introduction

The global construction sector is a major contributor to environmental pollution, responsible for approximately 40 % of global CO_2 emissions [1–3]. In response to these concerns, there is a growing need for sustainable construction practices, with timber and its products emerging as a promising alternative to traditional building materials like steel and concrete [3]. Timber not only reduces emissions during construction but also serves as a carbon sink throughout its lifecycle. Engineered Wood Products (EWPs), such as Cross-Laminated Timber (CLT) and Glued-Laminated timber (Glulam), offer significant carbon storage potential [4–6]. This property classifies timber as a carbon-negative material, fuelling its increasing popularity in construction worldwide. Beyond environmental benefits, timber construction offers advantages such as quicker prefabrication, a lighter structural weight suited for challenging sites such as vertical additions to existing buildings, and healthier indoor environments [7]. However, timber floors, especially lightweight long-span systems, are particularly vulnerable to excessive vibrations caused by everyday human activities, such as walking, which can be problematic in modern open-plan buildings. Consequently, there is a need to refocus design priorities from ultimate limit states to serviceability limit states, with particular emphasis on vibration control to enhance occupant comfort [8].

Extensive research has focused on defining vibration criteria and developing design approaches to improve the vibration serviceability of timber floors. Early research by Reiher and Meister [9] established that the perception threshold for steady-state vibrations is primarily governed by vibration velocity. Subsequent studies by Postlethwaite [10] and King [11] suggested that for frequencies below 10 Hz, acceleration correlates more strongly with the perception threshold than velocity. On the other hand, Lenzen [12] argued that steady-state perception thresholds are not directly applicable to building occupants, emphasising the need for alternative evaluation criteria. Wiss and Parmalee [13] later demonstrated that transient vibrations become less perceptible

with increased damping. To further refine the criteria for occupant comfort, Smith and Chui [14] introduced the concept that vibration limits should consider both frequency and root mean square (rms) acceleration.

Further research by Howarth and Griffin [15] highlighted that annoyance levels increase with the frequency of vibration-inducing events. This was reinforced by Ljunggren [16], who found that annoyance escalates when multiple frequency components are involved. For assessing transient vibrations, Ellis [17] and Griffin [18] advocated for the use of cumulative measures, such as the Vibration Dose Value (VDV), as a more appropriate metric for assessing comfort. A notable contribution from Toratti and Talja [19] introduced a five-class classification system for floors, each with specific vibration criteria. Hamm et al. [20] also provided practical guidelines for designing timber floors that minimize vibration issues, based on both laboratory experiments and real-building measurements.

However, deterministic walking force models have shown inconsistencies in predicting floor vibration responses, as noted by Brownjohn [21,22], Racic [23,24], and Chen [25]. To address this issue, Chang et al. [26] proposed a novel design method that aligns with current practices and is specifically tailored for timber floors. These findings have influenced the development of various standards and guidelines to addressing vibration serviceability, including Australian Standard AS/NZS 1170.0 [27], BS 6472–1 [28], CSA 086:19 (National Standard of Canada) [29], Eurocode 5–1–1:2004 [30], ISO 10137 [31], and the JRC–ECCS Joint Report (JRC 55118) [32]. Additionally, industry guidelines such as the AISC Design Guide 11 (DG 11) [33], the Steel Construction Institute's SCI P354 [34], the Cement and Concrete Industry's CCIP-016 [35], and the HIVOSS One Step Root Mean Square (OS-RMS) method further inform the design and evaluation of timber floors in terms of vibration serviceability [36].

Vibration serviceability assessment of timber floors depends not only on their structural properties but also on human perception of these vibrations. While most research, standards, and guidelines focus on timber floors with spans up to 7 m, there is a significant gap in established vibration criteria for lightweight, long-span timber floors [7]. Despite meeting the existing standards and guidelines, long-span timber floors often receive unfavourable feedback regarding their vibration serviceability [7]. One promising solution is the steel-wood timber truss (SWTT) floor panel system, which combines steel-wood timber trusses with particleboard panels. This system offers several advantages, including the ability to design large open spaces, enhance on-site construction efficiency, and promote sustainability through the ease of assembly, dismantling, and recycling of prefabricated components at the end of their service life. This study investigates the vibration performance of an 8-meter-long lightweight timber floor—representing a long-span configuration for commercial applications. Despite increasing interest in timber construction, there remains a lack of experimental data on the dynamic behaviour of long-span lightweight floor systems. The research combines experimental testing under various configurations (including variations in particleboard thickness and the use of strongbacks) with numerical modelling to capture static deflection, modal properties, and dynamic response. Additionally, human perception of vibration was assessed using both in-person walking trials and virtual reality environments, making this one of the first studies of its kind conducted in Australia. The main objective is to establish an experimental foundation for future research and industry practice by evaluating the effectiveness of different design parameters, analysing user comfort, and comparing current international design guidelines in light of the measured data and perception surveys. While SWTT systems have been previously used in floor spans up to 6 m, this study explores their application for extended spans of 8 m, where vibration serviceability becomes a critical concern. The novelty of this work lies not in the invention of a new system, but in the systematic experimental and numerical evaluation of an existing system beyond its conventional design scope. This includes the integration of strongbacks as a retrofit measure, assessment through combined modal testing and numerical simulation, and the correlation of results with human perception surveys. The objective is to establish a performance-based framework for future design and guideline refinement specific to LSTFs.

The floor system is defined in Section 2. Experimental and finite element analysis (FEA) studies of static and dynamic properties of the SWTT joists and the LSTF floor system are presented in Sections 3 and 4, respectively. In Section 5 a comprehensive assessment of the design of the floor system without strongbacks to international standards and guidelines for timber floor vibration is provided. Walking excitation experiments and the survey of participants for perception of vibration of the floor system with and without strongbacks are discussed in Section 6.

2. The floor system and test configurations

The floor system, measuring 2400 mm (in width) $\times$ 8000 mm (in length), is commonly used in low-rise residential and commercial buildings across Australia, as depicted in Fig. 1 and Fig. 2. This system consists of either a 19 mm thick particleboard (PB19 Structa Yellow tongue) or a 25 mm thick particleboard (PB 25 Structa Blue tongue) slab, which is glued and screwed to 6 $\times$ SWTT, also known as joists. For reference, a typical 200 mm-thick simply supported reinforced concrete slab spanning 8 m has a self-weight of approximately 500 kg/m^2, whereas the LSTF system presented in this study weighs only about 120 kg/m^2 emphasizing its lightweight advantage. The truss joists have a height of 660 mm spaced 450 mm centre-to-centre and are made up of Machine Graded Pine (MGP12) lumbers in top and bottom chords measuring 90 mm (width) $\times$ 45 mm (thickness) and MGP10 measuring 90 mm (width) $\times$ 35 mm (thickness) in the vertical studs. Commercial steel diagonals Steel-Wood 660–35 components with a C-shaped cross-section, 1 mm in thickness are connected to the timber joists via 1 mm thick steel nail plates. The system is supported along two edges by MGP12 bearer beams measuring 90 mm (width) $\times$ 45 mm (thickness), which are mounted on 360 Parallel Flange Channel (PFC) steel beams with flange length and thickness of 100 mm and 15 mm, respectively and web length and thickness of 380 mm and 10 mm, respectively.

The strongbacks are laminated veneer lumbers (LVL) F17 grade, 300 mm (width) $\times$ 45 mm (thickness) in cross-section, each secured to every vertical stud with two 6 mm (diameter) $\times$ 60 mm (length) commercial type 17 batten screws. Material properties of lumber (MGP) and LVL (F), per the Australian Standard [37] and properties of steel taken from the Australian Standard [38] are represented in Table 1. In the table, ρ is density (kg/m^3), E_L, E_R and E_T denote the average moduli of elasticity (MPa) in directions parallel (L), radial (R), and perpendicular (T) to the grain, respectively; μ_{LR}, μ_{LT} and μ_{RT} indicate Poisson's ratios in the LR, LT and RT directions, respectively; and G_{LR}, G_{LT} and G_{RT} are the shear moduli (MPa) in the LR, LT and RT directions, respectively. Particleboard (PB), being an isotropic material, has its mechanical properties determined through experimental testing based on ASTM D1037–12 [39] standard, as shown in Table 1. For the sake of brevity, the test procedure and load-deflection curves are not shown.

The following LSTF configurations (see Fig. 1 and Fig. 2) are constructed herein: (1) a system with a 19 mm subfloor particleboard and no strongback (NB19), (2) a system with a 25 mm subfloor particleboard and no strongback (NB25), (3) a system with a 25 mm subfloor particleboard and a single LVL strongback (1SB) in the mid-span, and (4) a system with a 25 mm subfloor particleboard and three LVL strongbacks (3SB) at middle and one-fourth span positions. The NB19 and NB25 tests are planned to investigate the effect of slab thickness on the dynamic properties of the LSTF, whereas 1SB and 3SB tests are performed to investigate dynamic properties, response to walking excitations, codified design comparison and human perception analyses of the LSTFs.
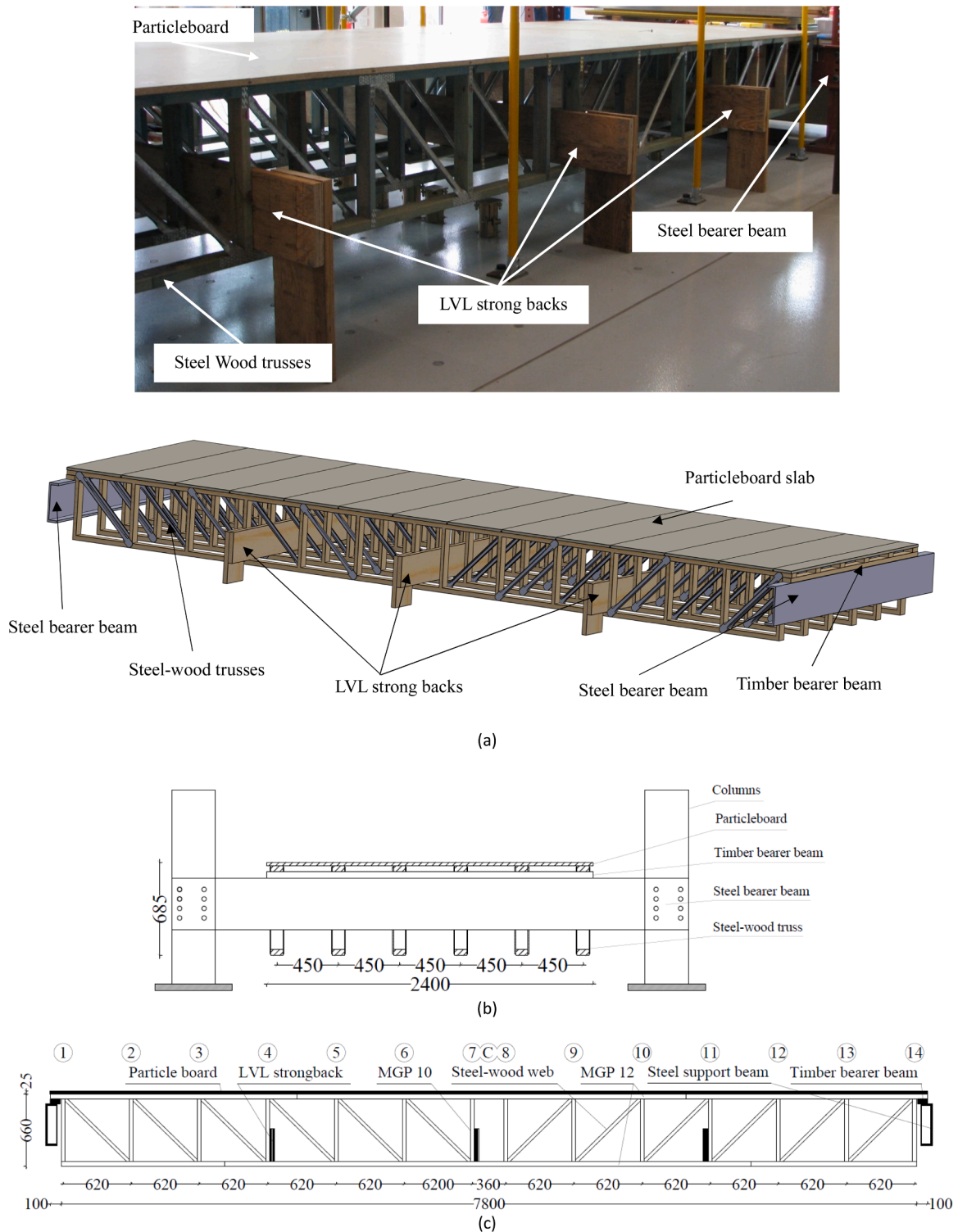
Fig. 1. The simply supported LSTF floor system showing: (a) floor setup and its components, (b) front-rear elevation, (c) side elevation, all units are in mm.

## 3. Static and dynamic properties of the steel-wood timber truss

This section contains the experimental and finite element analyses (FEA) assessment of the static and dynamic response of SWTTs. A total of 10 trusses were manufactured and tested under static loading and experimental modal analyses (EMA). The FE models of the LSTF were calibrated in two stages: first, using the results of static load tests to refine stiffness-related parameters, and second, by comparing numerical modal analysis (NMA) outcomes with experimental modal analysis

(EMA) measurements to validate and adjust the dynamic characteristics of the model.

3.1. Static 1 kN test of the SWTT

Each truss was assembled in a simply supported configuration (pin at left and roller at the right end) and a 1 kN load was applied at the centre. As shown in Fig. 3b, the load was gradually applied on the top chord directly above the vertical studs as well as at the centre of each truss. The
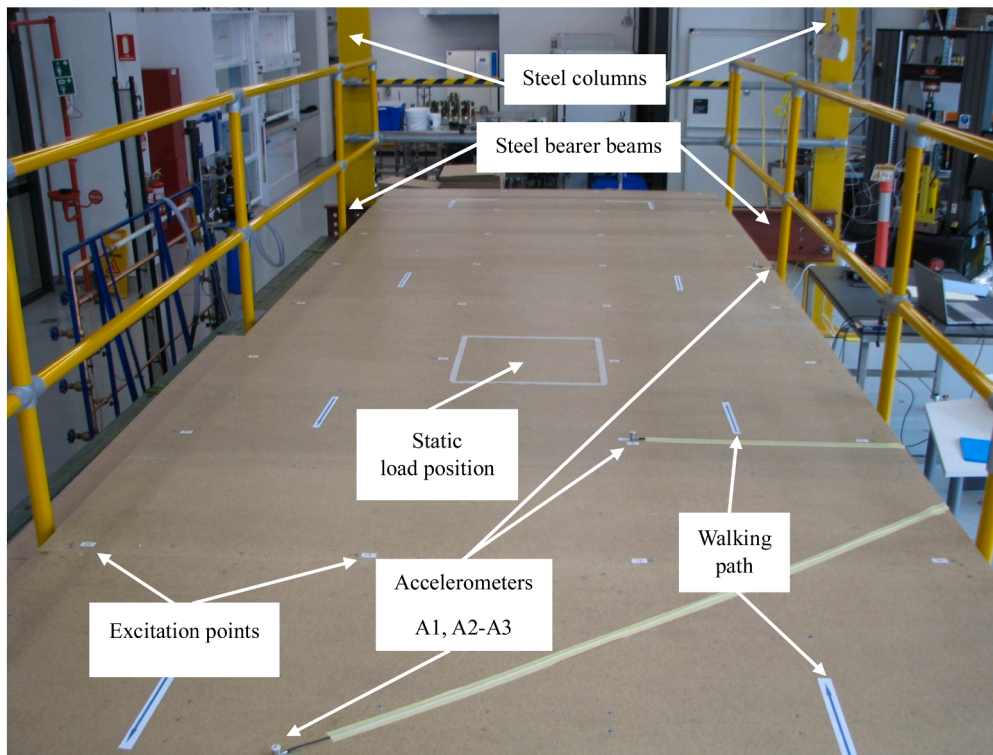
Fig. 2. Plan layout, showing the walking path, locations of the accelerometers A1, A2 and A3 (red circles), laser detectors L1- L9 (green circles), static load position (square at centre), and hammer excitation points 1–44 (black dots). All units are in mm.

Table 1
Mechanical properties of the floor system components.

Material	ρ (kg/m³)	E_L (MPa)	E_R (MPa)	E_T (MPa)	μ_{LR}	μ_{LT}	μ_{RT}	G_{LR} (MPa)	G_{LT} (MPa)	G_{RT} (MPa)
MGP10	565	10,000	780	1130	0.292	0.382	0.328	820	810	130
MGP12	575	12,000	936	1356	0.292	0.382	0.328	984	972	156
F17	650	14,000	1092	1582	0.292	0.382	0.328	1148	1134	182
PB19	685 (0.4 %)	4850 (0.2 %)	4850	4850	0.103	0.103	0.103	1877	1877	1877
PB25	706 (0.6 %)	4140 (0.1 %)	4140	4140	0.130	0.130	0.130	1877	1877	1877
Steel	7850	200,000	200,000	200,000	0.25	0.25	0.25	80,000	80,000	80,000

*Coefficient of variation (CoV) on measurements given in bracket next to each average value.

deflection directly under the load was measured using an optical laser displacement sensor (Panasonic HG-C1100) with a precision of 0.01 mm, underneath the bottom chord. Fig. 3c also shows schematic contour plot of the vertical deflection in the truss from a static FEA. The FEA method will be explained in detail in Section 4.1. The average measured experimental deflection (δ_{SWTT}^E), and that of the FEA (δ_{SWTT}^F), are given in Table 2 and are shown to be only 1.82% different across all 10 tests. It should be noted that for a confident verification of the FEA, the 1 kN was moved along the top chord from station 1–14 (see Fig. 3a) and corresponding deflections under the load at each station were
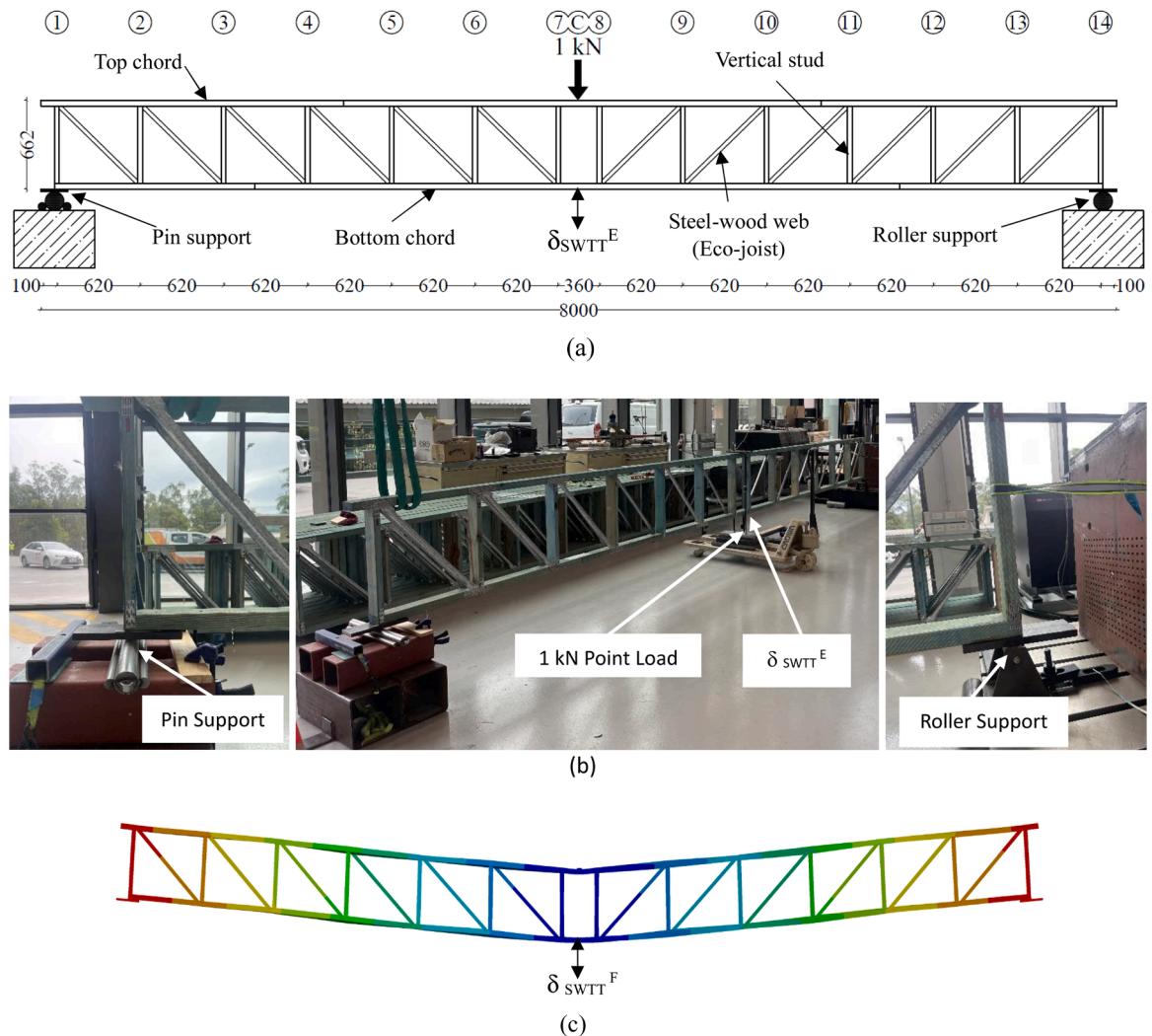
Fig. 3. Static 1 kN load tests of the 8m long SWTTs showing; (a) schematic drawing of SWTT, (b) the experimental setup, and (c) the FEA vertical deflection contour.

Table 2

Average measured static deflection versus FEA estimate under 1 kN load applied in the mid-span.

FEA δ_{SWTT}^F (mm)	Exp. δ_{SWTT}^E (mm)	Difference (%)
2.87	2.93 (1 %)	1.82

*CoV of 10 tests is given in brackets for the average measurement.

measured. The experimental and FEA results were in good agreement. However, these results are not the focus of the current study and are not presented herein.

3.2. Modal analysis of the SWTT

The test setup is shown in Fig. 4. Trusses were suspended at two ends by attaching slings to the top chord. Each truss was excited at 28 locations (see Fig. 4b) using an instrumented hammer (IEPE Brüel & Kjær type 8206), with each point being hit three times to ensure repeatability. Two tri-axial accelerometers (356A16), AC1 and AC2, were mounted on the top and bottom chords and near the left support, while a single-axis accelerometer (352C33), AC3, was positioned on the side of the top chord near the right support as depicted in Fig. 4b. The Frequency Response Functions (FRFs) were obtained using a dynamic signal analyser, which measured the input excitation force and the corresponding output acceleration response at various sensor locations. The analyser processed this data in real-time to generate the FRFs used in the experimental modal analysis.

During the experimental modal analysis (EMA), the SWTT was not laterally restrained, and therefore, lateral out-of-plane motions were not physically constrained in the test setup. However, in the post-processing of the frequency response functions, we excluded lateral modes from the analysis to focus solely on the vertical vibration characteristics relevant to floor performance and occupant comfort. While several mode shapes were observed during both experimental and numerical modal analysis, only the major in-plane vertical bending modes were selected for further discussion and used in the calibration of the NMA. Specifically, the first (11.3 Hz) and third (37.2 Hz) in-plane bending modes from the FEA were matched to the corresponding experimental modes at 10.5 Hz and 36.8 Hz, respectively, with good agreement in both frequency and shape.

A detailed description of the EMA and NMA methodologies are reported in a previous article [7] by the corresponding author. The first two in-plane bending mode shapes of the SWTT from EMA and NMA are shown in Fig. 5. Frequencies and damping ratio (ζ) calculated using the half-bandwidth method [31,40] are represented in Table 3. The differences between the frequencies from EMA and NMA in Table 3 are less than 10 % and a good correlation between the numerical and experimental mode shapes can be seen in Fig. 5.
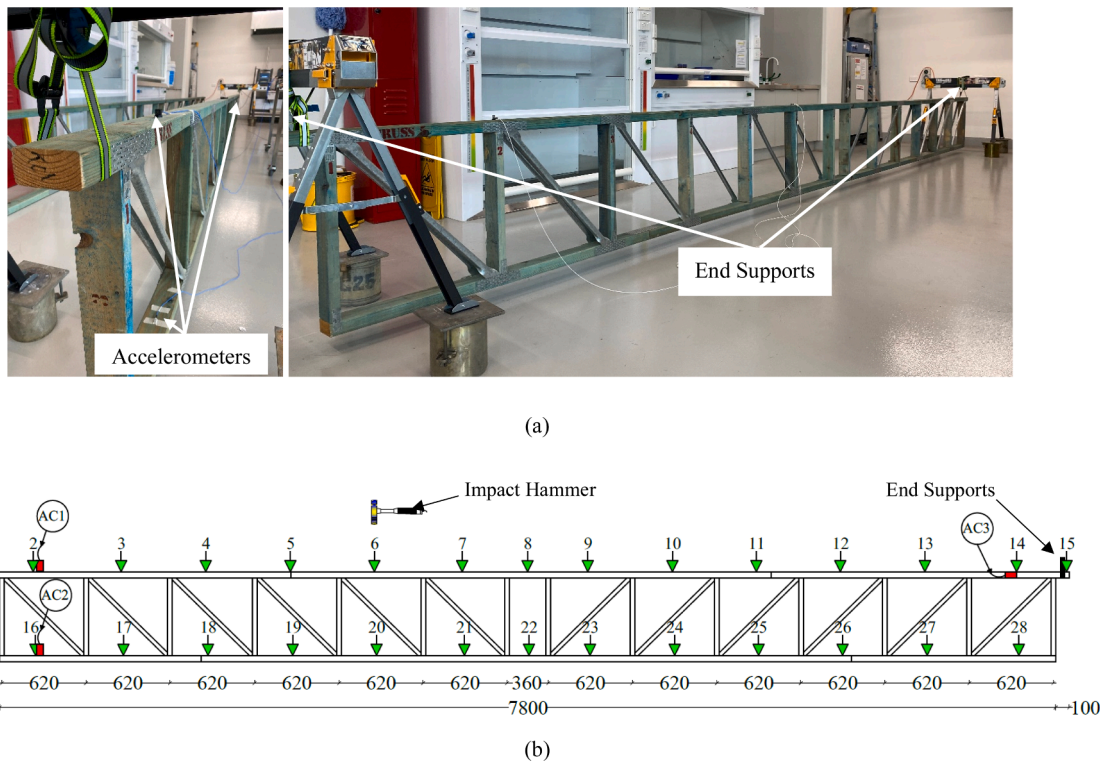
(a)

(b)

Fig. 4. Modal testing of the SWTT showing: (a) the test setup, and (b) the 28 hammer excitation points and accelerometer receivers (AC1-AC2-AC3).

f_{1E}^T=10.5 Hz

f_{1F}^T=11.3 Hz

f_{3E}^T=36.8 Hz

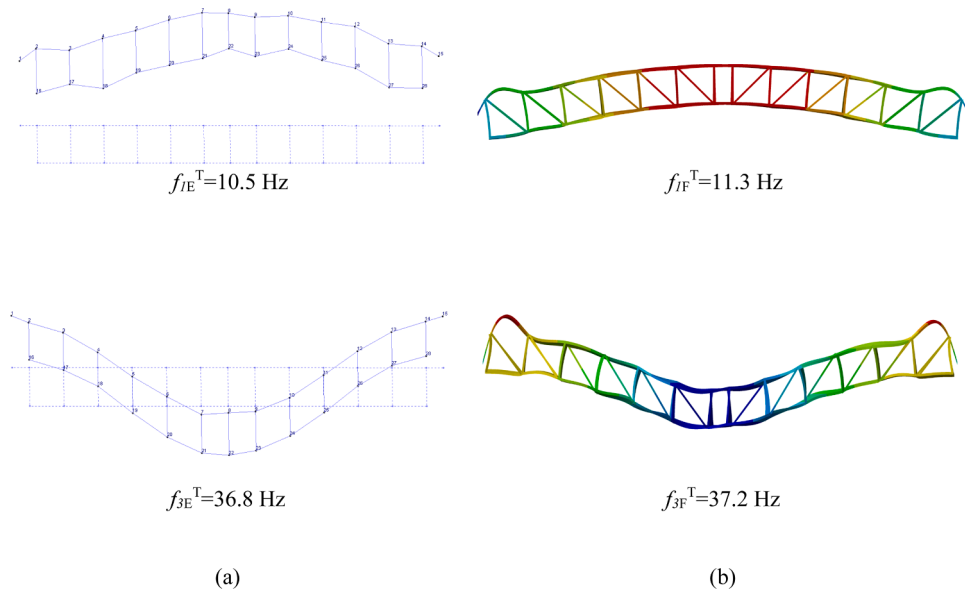f_{3F}^T=37.2 Hz

(a)

(b)

Fig. 5. (a) Experimental Modal Analysis (EMA), and (b) Numerical Modal Analysis (NMA) results showing the first two in-plane major bending mode shapes of the SWTT.

Table 3
Experimental modal analysis (EMA) and numerical modal analysis (NMA) results of the steel-wood timber truss (SWTT).

Mode shape (see Fig. 5)	FEA f_F^T (Hz)	EMA f_E^T (Hz)	ζ_{EMA} (%)
1	11.3	10.5	0.97
2	37.2	36.8	0.55

4. Static and dynamic properties of the floor system

4.1. The finite element model

The finite element mesh of the LSTF system modelled in ANSYS [41] is shown in Fig. 6. Top and bottom chords and vertical studs were modelled using 20-node SOLID186 elements with 6 degrees of freedom at each node. Corresponding MGP orthotropic material properties in
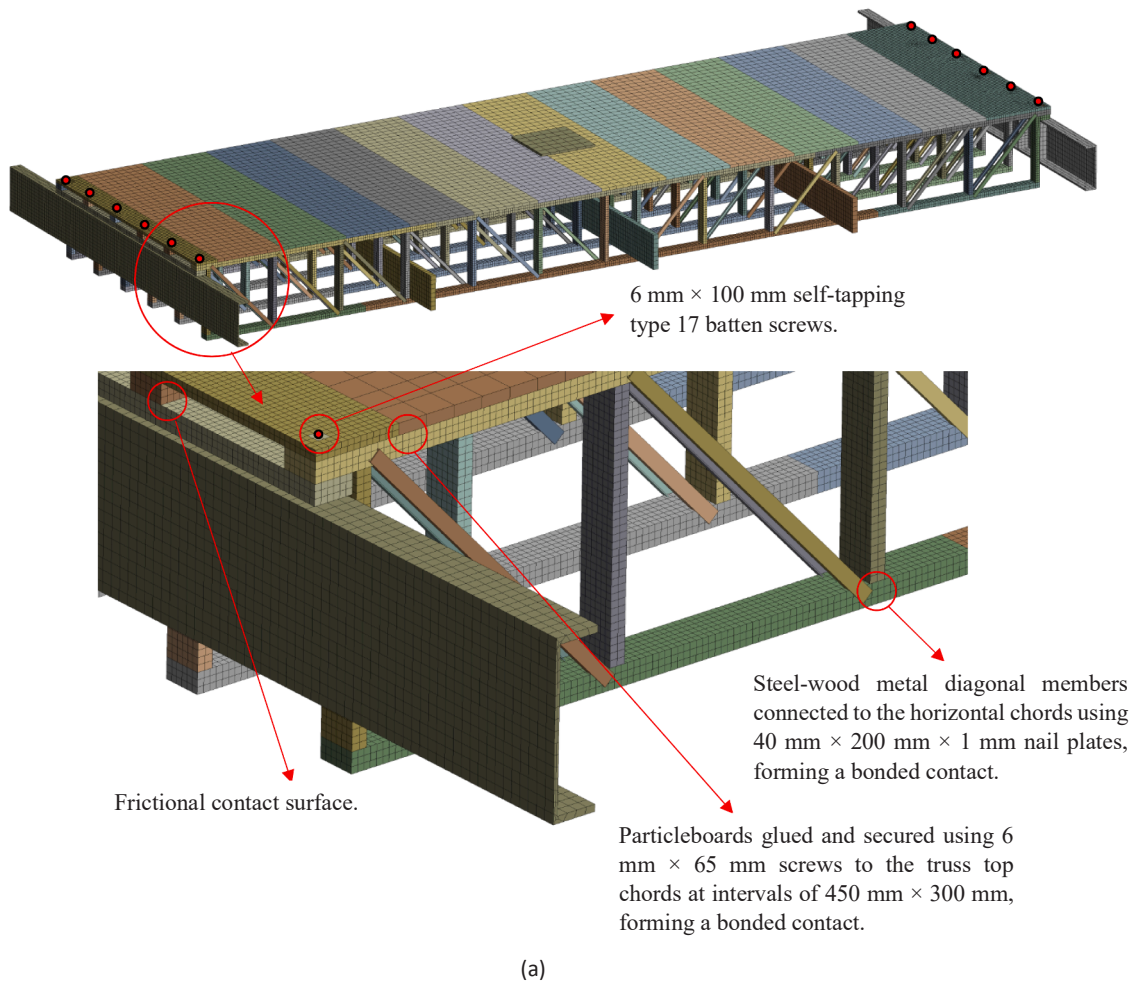
6 mm × 100 mm self-tapping type 17 batten screws.

Steel-wood metal diagonal members connected to the horizontal chords using 40 mm × 200 mm × 1 mm nail plates, forming a bonded contact.

Frictional contact surface.

Particleboards glued and secured using 6 mm × 65 mm screws to the truss top chords at intervals of 450 mm × 300 mm, forming a bonded contact.

(a)

Fig. 6. Finite Element Mesh of the lightweight long-span timber floor (LSTF) system.

Table 1 were assigned to these elements. The particleboard and PFC steel bearer beams were also meshed using SOLID 186 elements with isotropic material properties given in Table 1. Steel diagonals Steel-Wood 660–35 components were modelled using LINK 180 tension/compression-only elements [42]. The steel nail plate was not modelled, and the diagonal-to-timber chord connection was modelled using bonded contact in ANSYS [42]. All other contact surfaces were modelled using frictional contact formulation with a coefficient of friction of 0.45 for the timber-steel interface and 0.32 for the timber-timber interface (calculated from simple laboratory tests). Commercial type 17 batten screws with a length of 100 mm and diameter of 6 mm were modelled using BEAM 188 elements with corresponding steel properties and equivalent net area. The centre of the fastener was connected to the surrounding solid elements by using multipoint constraint contact (MPC) elements [42]. To accurately model the screw withdrawal capacity, FEA model was created and validated against the experimental tests of [43]. A comprehensive explanation of the FEA modelling of the screw and its validation is given in [44].

4.1.1. Finite element model calibration

To ensure the accuracy of the FE model, a two-stage calibration process was carried out based on static deflection results and EMA. Bonded contacts were initially defined between timber-to-steel and timber-to-timber interfaces. After comparing results with static deflection, these were subsequently replaced with frictional contacts, using coefficients of friction obtained from laboratory tests. A penalty-based contact stiffness formulation was employed. Sensitivity analyses were

carried out to ensure that excessive interface stiffness did not artificially reduce global deflection. Default ANSYS penalty stiffness values were used as a baseline and then manually adjusted by up to 20 % during calibration. The model was considered calibrated when the predicted mid-span deflections matched the experimental results within 10 %.

The interface between the timber chords and the steel bearer beams was initially modelled using bonded contact to represent shear transfer. This was later replaced with an explicit screw-based connection model, allowing for vertical slip through frictional contact. The screw fasteners were modelled using BEAM188 elements, with their positions and diameters accurately represented. These were connected to the surrounding solid mesh (particleboard, timber chords, and steel bearer beams) using MPC elements to accurately represent load transfer.

For dynamic calibration, the EMA results of the NB25 system were used to refine boundary conditions in NMA. The floor was supported by steel bearer beams and simulated in ANSYS using bonded contact at the timber-steel interfaces, while the ends of the steel beams were modelled as fixed supports. The flooring system was considered in-plane free and vertically supported. Mode shapes and natural frequencies from the NMA were compared with those from EMA. Discrepancies led to refinement of the screw modelling and frictional definitions at joist-bearer and truss-end locations. After calibration, the fundamental frequency of the NB25 system matched the EMA result within 5 %, and good agreement in mode shapes was achieved.

4.1.2. Finite element mesh sensitivity

To understand the effect of mesh size on the results, FE models with

uniform element sizes of 15, 20, 25, 30, and 35 mm were created. Results for the mid-span deflection and the frequencies of the first three modes obtained from models with different mesh sizes indicated that a 20 mm mesh size provides an optimal balance between the solution accuracy and the computational efficiency. Frequency differences between the 15 mm and 20 mm mesh sizes were less than 1 %. Similarly, the differences in the mid-span deflection based on these mesh sizes were less than 4 %, confirming that the 20 mm mesh size was an ideal choice.

To ensure consistency between static and modal analyses, the same finite element geometry and mesh were used in both cases. However, the modal analysis was performed using the Block Lanczos method in ANSYS [41], which requires a fully linearised stiffness matrix. All contact pairs were assumed to be fully closed in the undeformed, zero-load configuration; this was enforced by setting appropriate contact offsets and surface positions during meshing so that the initial gap was zero. In this context, contact elements were linearised about their initial state, and no status changes (e.g., opening, closing, or slip) were permitted during eigenvalue extraction. Similarly, COMBIN39 elements used to model screw fasteners were defined by their linear axial stiffness (K1) only, with nonlinear effects such as slip or plasticity deactivated in modal analysis.

4.2. Static properties of the floor systems

A common practice for limiting the maximum deflection of floor panels under concentrated live loads has become widely accepted in addressing timber floor vibration concerns [7]. As outlined in ISO 18324 [45] and AS 1170.0 [46], mid-span deflections of the floor systems were measured by applying concentrated loads of 1 kN and 2 kN, as shown in Figs. 7a and 7b. To obtain a profile of the deformed shape, multiple optical laser displacement sensors (Panasonic HG-C1100) with a precision of 0.01 mm were positioned under the floor system (see Figs. 7c and 7d). The deflection was measured through the reflection of the laser beam from a soft board attached underneath the point of interest (particle board or bottom timber chord) at specific monitoring points on trusses T2, T3, T4, and T5 as shown in Fig. 2 with L1-L9. These points included the centre of the bottom chord of the mentioned SWTTs, the centre of the SWTT floor panels, and 1/3 of the span from each end of SWTT in T3 and T4, as illustrated by the green dots in Fig. 2.

The mid-span deflections under 1 kN and 2 kN concentrated loads from the experiment, Δ^E (measurement from L5 in Fig. 2 located at the centre of the floor), and the finite element analysis, Δ^F, are represented in Table 4 for four different tested floor systems. The experimental results represent an average of three test repeats and the corresponding CoV is shown in brackets. A maximum difference of 11.5 % between the experimental and FEA results in 1SB under 1 kN is observed. Differences under 2 kN load are less than 8.6 %. It should be noted that the deformed profile of the floor systems obtained from FEA was compared against all measurement readings at L1 to L9 and a good agreement was observed. This is not shown here for the sake of brevity.

To calculate the improvement in stiffness of the floor system by thickening the particleboard or introducing the strongbacks, static stiffening ratios are calculated by dividing the measured deformation of each floor system by that of the NB19 (19 mm particleboard without strongback). As shown in Table 4, increasing the thickness of the particleboard in the floors without strongbacks can enhance the stiffness by 5 % under 1 kN and 9 % under 2 kN loads. However, introducing a
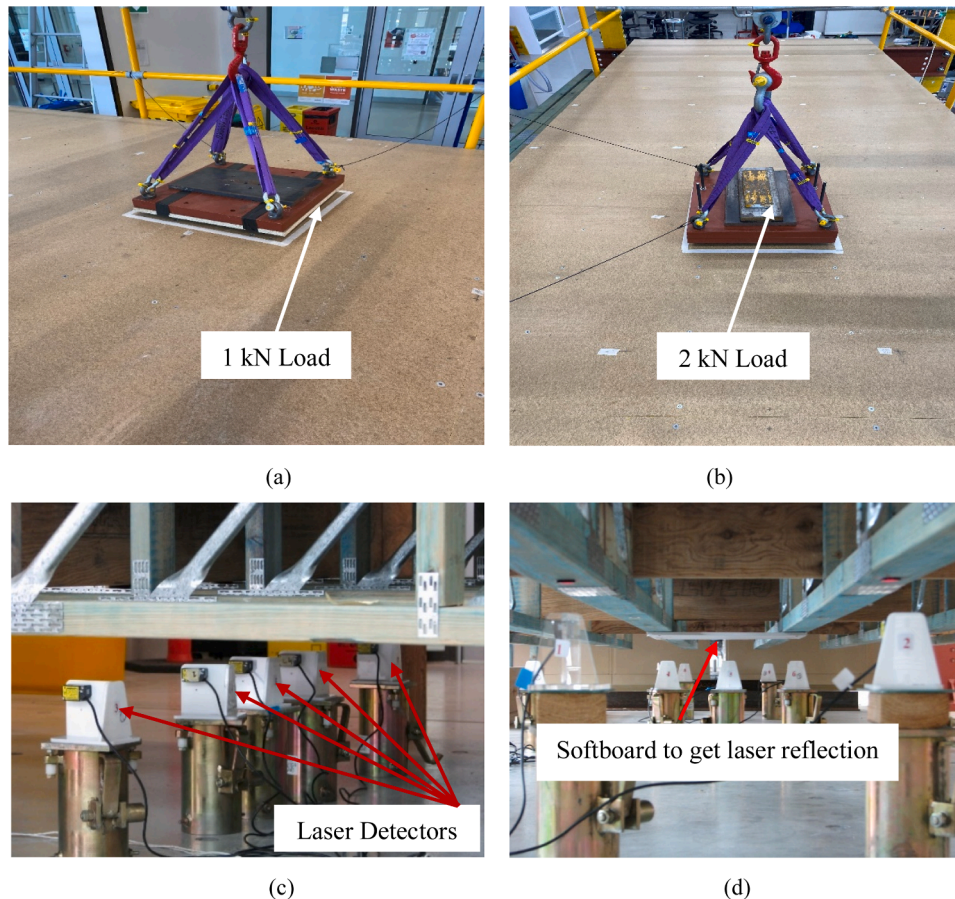
Fig. 7. Static mid-span deflection tests of the floor system showing; (a) applied static load of 1 kN, (b) applied static load of 2 kN, (c) laser detectors located underneath the floor panel, and (d) attached softboard to measure the deflection Δ^E.

Table 4
Static properties of the tested floor systems under concentrated mid-span load; Experiment vs. FEA.

Floor system	Particleboard thickness (mm)	No. of strongbacks	Exp.		FEA		Difference*		Static Stiffening Ratios	
			Δ_1^E 1 kN (mm)	Δ_2^E 2 kN (mm)	Δ_1^F 1 kN (mm)	Δ_2^F 2 kN (mm)	1 kN (%)	2 kN (%)	$\Delta_{1\text{-NB19}}^E$ divided by Δ_1^E	$\Delta_{2\text{-NB19}}^E$ divided by Δ_2^E
NB19	19	Nil	0.69 (1%)	1.40 (1%)	0.64	1.28	7.1	8.6	100%	100%
NB25	25	Nil	0.66 (0%)	1.28 (0%)	0.59	1.18	10.1	7.7	105%	109%
1SB	25	1	0.25 (0%)	0.48 (0%)	0.22	0.44	11.5	7.0	276%	292%
3SB	25	3	0.21 (1%)	0.41 (1%)	0.19	0.38	8.1	6.6	329%	341%

Coefficient of variation (COV) on measurements given in bracket next to each average value from three tests repeats.
* Difference= (EMA-FEA)/EMA.

single strongback can improve the static stiffness by 276–292 % for 1 kN and 2 kN loads, respectively. The floor system with three strongbacks is 19 % stiffer than the floor with a single strongback under the 1 kN load.

4.3. Dynamic properties of the floor systems

The dynamic characteristics of the floor systems were determined through experimental testing conducted following ISO 18324 [45]. A grid of 44 equally spaced node points (4 × 11) was established on the floor surface to serve as excitation points, marked by black dots in Fig. 2. Vibration acceleration data was collected using three single-axis accelerometers (INV9828), which were strategically placed away from the centre of the floor panel to capture higher vibration modes. The accelerometers A1 to A3 are indicated by the red dots in Fig. 2. The experimental setup included an impact excitation device (digital hammer, IEPE Brüel & Kjær type 8206), a data acquisition instrument, and the accelerometers. To exclude the effect of the weight of the tester, a technician walked next to the floor panel, applying impact excitation with the instrumented hammer. The distribution of excitation points was displayed using the ECON Data Acquisition and Analysis System (MI-7008). Vertical vibrations recorded at the grid points were converted into electrical signals, which were continuously logged by the Modal Genius data acquisition system. These signals were then processed using Fast Fourier Transform (FFT) to obtain the Frequency Response Function (FRF). From the FRF, the modal frequencies, mode shapes, and damping ratios of the SWTT floor systems were extracted.

Mode shapes and frequencies of NB25 and 3SB are shown in Figs. 8 and 9, respectively. The contour legends show the normalised vertical deformation from NMA. Frequencies and damping ratios from EMA and NMA are represented in Table 5. Mode shapes are defined as *M(i,j)* where *i* denotes the number of lobes in the longitudinal direction and *j* corresponds to the number of lobes in the transverse direction. Damping is calculated using the −3 dB method recommended in ISO 10137 [31]. In general, there is a good agreement between the modal shapes and frequencies measured (EMA) and calculated (NMA). By introducing the strongbacks, the fundamental frequency corresponding to the bending mode changes from 15 Hz to 26.9 Hz, which is equivalent to an 80 % increase. Critical damping ratios vary in different modes and are between 0.7 % and 3.4 %, which agrees with previous research [7] and the standard/guideline recommendations for a bare floor (without imposed loads, furniture, partitions, etc). Comparison between mode shapes of the NB25 and 3SB floor systems shows that by introducing strongbacks into the floor system, all frequencies of the major bending modes are increased. Additionally, by using strongbacks the floor system depicts two-way bending behaviour as observed in the change in the mode shapes, particularly modes M (1,1) and M (2,1). The modal mass contributions in the vertical translation from the NMA are also shown in Table 5. It can be seen that in NB25 a total of 52.8 % mass is contributed to bending modes with frequencies between 15 Hz to 16.6 Hz. It should be noted that modes M(1,2) and M*(1,1) were not observed in the EMA, although they were predicted by the NMA. This discrepancy is likely due to the close spacing of these modes in frequency and the limited number

of measurement points used (three accelerometers). In such cases, the resolution and reliability of the EMA results may be affected, particularly when nodal lines of undetected modes coincide with sensor positions or the excitation energy is insufficient to activate certain modal shapes. Nonetheless, their existence is supported by the numerical model. Future work should consider the inclusion of additional sensor locations and a broader set of excitation points to enhance the resolution and capture of such higher-order or spatially complex modes. In the 3SB floor, the fundamental bending mode has a mass contribution of 51.6 % and is quite distinctive from any other bending mode (see Fig. 9). Note that unlike NB25 which has a torsional mode shown with M(0,0) in Fig. 8, no torsional modes were observed in 3SB within the studied frequency range.

5. Vibration serviceability assessment of NB25 floor system according to international standards and guidelines

The design and acceptability of the simply supported 8 m NB25 floor system used in a commercial building are compared to the recommendations in different international standards and guidelines. The following methods are commonly used to ensure a floor system meets vibration serviceability criteria: (1) static deflection methods in AS 1170.0 [27] and International Residential Code (IRC) [47], (2) frequency-deflection check in ISO/TR 21136 [48], EN 1995–1–1 [30], CSA 086:19 [29], HIVOSS (OS-RMS) [49], and (3) modal method in AISC/DG11 [33], SCI P354 [34], and CCIP016 [35]. A comprehensive discussion of these methods is given in [7] and this section is dedicated to a comparison between the vibration prediction and acceptability of NB25.

### 5.1. Static deflection methods

Static deflections of the NB25 under 1 kN and 2 kN, as represented by that experimental measurements in Table 4, are less than the 2 mm limit recommended in AS 1170.0 [27]. Under a combined self-weight and 40 % live load, with distributed live loads of 3 kPa for commercial buildings, deflection calculated from FEA is 13.4 mm which is lower than the 26.7 mm (L/300) criterion recommended in AS 1170.0 [27] suggesting that NB25 is compliant.

The static deflection criteria in IRC [47] for mixed-use dwellings is L/360 (22.2 mm) under 40 psf (1.91 kPa) live load. The static deflection of NB25 from the FEA is 16.9 mm confirming that the floor is acceptable.
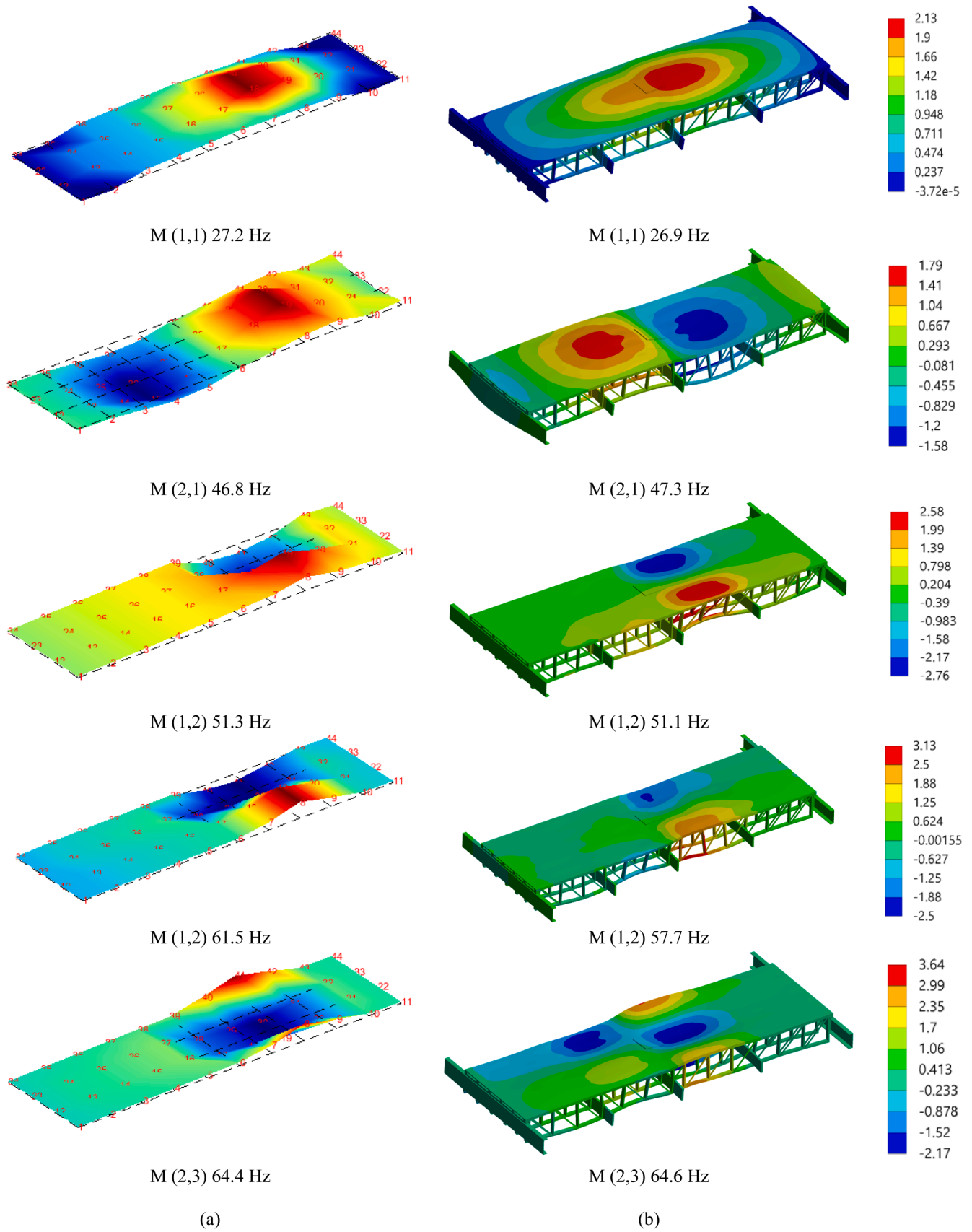
5.2. Frequency-deflection methods

Empirical and simplified analytical approaches are frequently utilised in vibration design to correlate a floor's fundamental frequency with its static deflection [48]. The simplified method outlined in ISO/TR 21136 [48] recommends the following relationship:

$$\frac{f^{2.56}}{d_1} \geq 1{,}090.31 \tag{1}$$
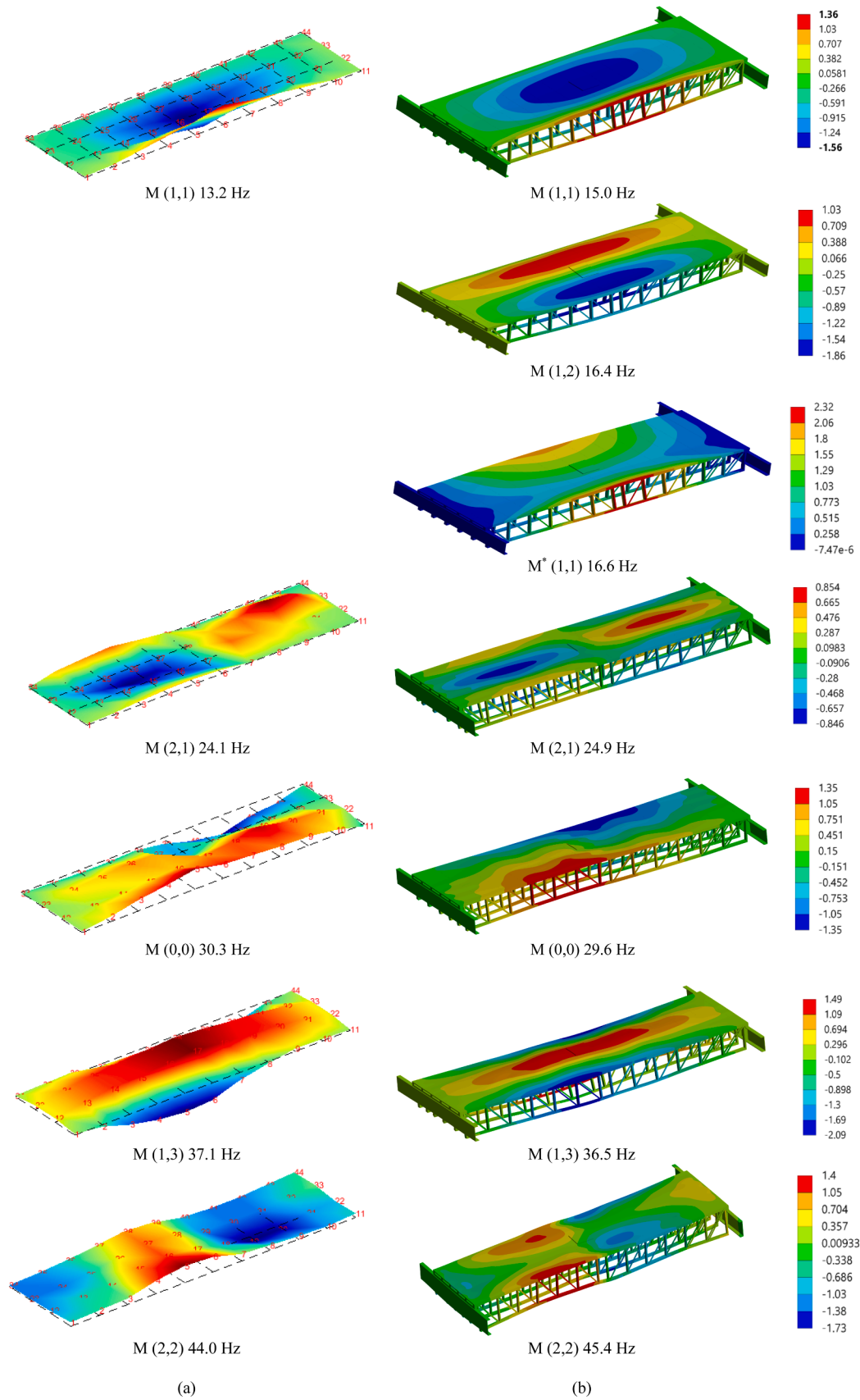
Fig. 8. Dynamic properties of the NB25 floor system showing mode shapes and frequencies of (a) EMA and (b) NMA.

M (1,1) 27.2 Hz   M (1,1) 26.9 Hz

M (2,1) 46.8 Hz   M (2,1) 47.3 Hz

M (1,2) 51.3 Hz   M (1,2) 51.1 Hz

M (1,2) 61.5 Hz   M (1,2) 57.7 Hz

M (2,3) 64.4 Hz   M (2,3) 64.6 Hz

(a)   (b)

Fig. 9. Dynamic properties of the 3SB floor system showing mode shapes and frequencies from (a) EMA and (b) NMA.

Table 5
Dynamic properties of NB25 and 3SB from EMA and NMA.

Mode	NB25 (Fig. 7)				Mode	3SB (Fig. 8)			
	f^{NMA} (Hz)	f^{EMA} (Hz)	ζ (%)	Modal mass contribution**		f^{NMA} (Hz)	f^{EMA} (Hz)	ζ (%)	Modal mass contribution**
M (1,1)	15.0	13.2	3.4	14.4 %	M (1,1)	26.9	27.2	2.2	51.6 %
M (1,2)	16.4	-	-	3.8 %	M (2,1)	47.3	46.8	1.4	0.12 %
M* (1,1)	16.6	-	-	34.6 %	M (1,2)	51.1	51.3	1.6	0.01 %
M (2,1)	24.9	24.1	2.1	0.01 %	M (1,2)	57.7	61.5	1.7	0.01 %
M (0,0)	29.6	30.3	0.7	0.01 %	M (2,3)	64.6	64.4	1.1	0.7 %
M (1,3)	36.5	37.1	2.2	0.01 %					
M (2,2)	45.4	44.0	1.3	0.01 %					

* Duplicate mode.
** Mass contributions correspond to translation in the vertical direction calculated from FEA.

where d_1 is the measured 1 kN point load deflection in mm and f is the measured floor fundamental natural frequency in Hz. Based on the measured deflections and frequencies in Tables 4 and 5, the ratio on the left-hand side of Eq. (1) is equal to 1,120 for NB25 which satisfies the condition.

EN 1995–1–1 [30] recommends three criteria (i), (ii), and (iii) for timber floors:

$$f > 8Hz \quad \text{(i)} \qquad f = \frac{\pi}{2L^2}\sqrt{\frac{(EI)_L}{m}}$$

$$\frac{d}{F_s} \leq a \quad \text{(ii)} \qquad v = \frac{4(0.4 + 0.6n_{40})}{mbL + 200} \qquad (2)$$

$$v \leq b^{(f\xi-1)} \quad \text{(iii)} \quad n_{40} = \left\{ \left(\left(\frac{40}{f}\right)^2 - 1 \right) \left(\frac{b}{L}\right)^4 \frac{(EI)_L}{(EI)_b} \right\}^{0.25}$$

where m represents the mass per unit area (kg/m²), L and b denote the span and width (m) respectively, and v is the maximum initial vertical velocity (m/s) resulting from an ideal unit impulse (1 Ns) applied at the floor location that induces the maximum response. The first criterion is satisfied since the fundamental frequency of NB25 (13.2 Hz) is larger than 8 Hz. Using FEA, the bending stiffness of a 1-meter-wide panel in the longitudinal and cross-span directions is calculated as $EI/L = 1.71 \times 10^7$ Nm²/m and $EI/b = 2.77 \times 10^3$ Nm²/m, respectively. The number of first-order modes with natural frequencies of up to 40 Hz (n_{40}) is equal to 2 (see Fig. 8) and the unit impulse velocity response is found to be $v = 5.9$ mm/Ns². The fundamental frequency from Eq. (2) is determined to be 13.85 Hz which is in good agreement with the EMA/NMA frequencies in Table 5. The deflection-to-force ratio d/F_s is equal to 0.66 (under 1 kN load) and 0.64 (under 2 kN). Referring to EN 1995–1–1 [30], this places the floor well within the "better performance" region (Region 1), even when considering relatively high limiting values for a. Therefore, the outcome is robust across a wide range of national selections, and a direct comparison with any specific National Annex is not necessary in this case.

CSA O86:19 [29] suggests a vibration-controlled span limit (l_v) given by Eq. (3) for checking the vibration performance of joisted timber floors:

$$l_v = \frac{0.122(EI_{eff})^{0.284}}{k_{tss}^{0.14}m_L} \qquad (3)$$

$$k_{tss} = 0.0294 + 0.536k_1^{0.25} + 0.516k_1^{0.5} + 0.31k_1^{0.75}$$

where m_L is the mass per unit length (kg/m) of the floor system, EI_{eff} represents the effective flexural stiffness of the floor system in the span direction, k_{tss} is the factor accounting for the flexural stiffness in the transverse direction for k_1 (longitudinal stiffness factor). The parameters k_1 and k_{tss} are determined to be 0.19 and 0.52, respectively, while the EI_{eff} is calculated as 1.71×10^7 Nm² using FEA. By substituting in Eq. (3), l_v of 9,010 mm is calculated suggesting that an 8 m span is acceptable.

The One Step Root Mean Square (OS-RMS) method, as outlined in the Human Induced Vibration of Steel Structures (HIVOSS) [36] classifies the floor from the provided design diagrams from A to F. Using a recommended damping ratio of 3 % which is close to the measured damping in Table 5, frequency of 13.2 Hz and modal mass of 170 kg (m*=m/4), the OS-RMS90 analysis classifies NB25 within the E class [7]. According to HIVOSS [36] a class E floor is not recommended for critical workspaces, healthcare facilities, or educational buildings. It is considered marginal for residential, office, retail, hotel, and meeting room applications.

5.3. Modal superposition methods

While the methods discussed in the previous section can provide a quick guide for checking the, they lack accuracy [7]. Modal superposition methods incorporate detailed dynamic characteristics of the floor and have been shown to predict response parameters, such as velocity and acceleration under walking excitations, with greater accuracy than simplified approaches.

AISC/CISC Design Guide 11 (DG 11) [33] assesses the acceptability of high-frequency floors ($f > 9$ Hz) based on the calculated equivalent sinusoidal peak acceleration (a_{ESPA}/g), which represents the perceived response under walking excitation.

$$\frac{a_{ESPA}}{g} = \left(\frac{154}{M}\right)\left(\frac{f_w^{1.43}}{f_n^{0.3}}\right)\sqrt{\frac{1 - e^{-4\pi h\xi}}{\pi h\xi}} \qquad (4)$$

where M is the mass of the floor in lb and h is the walking frequency

harmonic matching the natural frequency equal to 7 for fundamental frequencies in the range of 13.2–15.4 Hz (note that the measured fundamental frequency of NB25 is 13.2 Hz). Assuming 3 % critical damping the peak acceleration (a_{ESPA}/g) ratio calculated from Eq. 4 ranges from 13 to 20 for walking frequencies 1.5 Hz $< f_w <$ 2.2 Hz. As recommended in AISC/CISC Design Guide 11 (DG 11) [33] the floor is deemed acceptable for office use at walking frequencies less than 1.6 Hz.

SCI P354 [34] recommends Eq. 5 to calculate the total acceleration response function, $a_{w(t)}$ of the floor for *N* modes of vibration and up to four harmonics of the modal force (f_h):

underestimation of actual response, especially in the presence of low damping and low mass systems. This reinforces our main point: while CCIP-016 [35] can be a useful tool, it should be applied with caution when assessing long-span timber floors, and further calibration for such systems is needed.

In contrast, the 3SB system (shown in Fig. 11c) displays a high-frequency response pattern, as seen in Fig. 10d. Due to the increased stiffness and fundamental frequency resulting from the installation of three strongbacks, the high-frequency assessment procedure of CCIP-016 [35] was applied. Fig. 11c shows the first bending mode used in the analysis, along with the identified excitation (E1 and E2) and

$$a_w(t) = \sum_{n=1}^{N} \sum_{h=1}^{H} \mu_{rn} \mu_{en} \frac{F_h}{m_n^*} \frac{h^2 \left(\frac{f_h}{f_n}\right)^2}{\sqrt{\left(1 - h^2 \left(\frac{f_h}{f_n}\right)^2\right)^2 + \left(2h\xi \left(\frac{f_h}{f_n}\right)\right)^2}} \sin(2\pi h f_h t + \phi_h + \phi_{nh}) W_b$$

$$\tan \phi_{nh} = \frac{-2h\left(\frac{f_h}{f_n}\right)\xi}{1 - \left(h\left(\frac{f_h}{f_n}\right)\right)^2} \quad -\pi \le \phi_{nh} \le 0$$

(5)

where $\varnothing_{nh}$ represents the phase shift of the response of the nth mode relative to the hth harmonic and μ_{rn} and μ_{en} are, respectively, the modal amplitudes of the response (*rn*) and excitation (*en*) points taken from the NMA for a floor with a total weight of W_b. Using N = 2 corresponding to modes M (1,1) and M* (1,1) associated with the largest modal mass contribution, an acceleration of 0.13 m/s^2 (1.3 %×g) corresponding to a response factor of 26 is calculated for NB25. Compared to the tolerance limits set by BS 6472–1 [28] and DG 11 [33], shown in Fig. 10a, the calculated acceleration does not meet the acceptability criteria for office buildings.

CCIP-016 [35] has two different methods for evaluating the response of the floor to walking excitations; (1) a method for low-frequency floors which exhibit a steady-state response, and (2) a method for high-frequency floors that is associated with transient response. The steady-state and transient responses are observed in NB25 and 3SB, shown in Figs. 10c and 10d, respectively for a brisk walking (f_w=2.2 Hz). The raw measured accelerations are filtered using the frequency weighting curves defined in BS 64721–1 [28] depicted in Fig. 10b.

In floors with steady-state response (see Fig. 10c) a harmonic method similar to SCI P354 [34] is suggested to calculate the acceleration response. The difference between SCI P354 [34] and CCIP-016 [35] is in the formulation of the harmonic force [7]. The CCIP-016 [35] method is explained in detail in [7]. The excitation points (E1 and E2) and response points (RO and RO$_c$) for calculation of the modal amplitudes μ_{rn}, μ_{en} are shown in Fig. 11a and correspond to the most critical locations based on the experimental walking paths in Fig. 2. The response factors (*RF*) of each walking frequency f_w, are plotted in Fig. 11b. It can be seen that the most critical *RF* corresponds to walking excitation closer to the edge of the floor when experienced by a receiver slightly offset from the centre of the floor. As shown in Fig. 11b, the calculated response factors of NB25 for the range of walking frequencies of a walker with a weight of 75 kg as recommended in CCIP-016 [35] are larger than the RF of 8 recommended for commercial floors [35]. This discrepancy is partly due to the fact that CCIP-016 [35] is primarily calibrated for concrete floors with natural frequencies below 10 Hz. In our study, we observed a clear resonance pattern for the NB25 floor, which justified the use of the CCIP-016 [35] approach as a first estimate for low-frequency excitation. However, the results highlight that applying CCIP-016 [35] directly to lightweight timber floors can lead to

response (R0 and R0c) locations. Fig. 11d presents a comparison between the predicted RFs and the measured values from W1 (denoted by *) over the same frequency range. For the 3SB system, the predicted RFs from all four excitation–response combinations (E.1, R.0 - E.1, R.0c and E.2, R.0 - E.2, R.0c) remained mostly below the RF limit of 8 across the walking frequencies. Similarly, the experimental RFs also remained below the threshold for most frequencies, confirming that the addition of strongbacks significantly reduced the vibration response. An exception was observed at f_w = 2.1 Hz, where the measured RF marginally exceeded the limit.

These results demonstrate that while the NB25 floor fails to meet vibration serviceability limits in its original configuration, the retrofitted 3SB system shows substantial improvement, successfully reducing both predicted and measured RFs to acceptable levels under most walking conditions.The use of the low-frequency method in evaluating response factors may appear questionable. However, it is important to note that the rationale behind applying the low-frequency (resonance) method in CCIP-016 [35] is based on the assumption of a steady-state floor response. Experimental measurements, such as the acceleration time history shown in Fig. 10c, indicate that the NB25 floor exhibits steady-state behaviour, thereby justifying the adoption of the low-frequency model.

6. Walking excitations and perception of the comfort of the floor system without strongbacks (NB25) and with three strongbacks (3SB)

### 6.1. Walking excitation measurements

This section examines the vibration performance of the NB25 and 3SB floor systems and the assessment of human perception of vibration from several experiments and surveys. The floors were tested to a single person walking along the path following the indicated direction of movement in red dashed line as shown in Fig. 2. Seven different walking frequencies (f_w) ranging from 1.60 Hz (normal walking) to 2.20 Hz (fast walking) were considered, with a metronome used to ensure accurate and consistent step timing. Three individuals participated in the testing: walker 1 (W1) weighed 75 kg (750 N), walker 2 (W2) weighed 80 kg (800 N), and walker 3 (W3) weighed 85 kg (850 N). All walkers

maintained a constant stride length of 700 mm at all walking speeds. W1 and W2 walked on the NB25 and W1 and W3 walked on 3SB floor. The weights of walkers were chosen based on the recommended weight range in different guidelines [7]. Accelerations were measured at A1 to A3 shown in Fig. 2. A Butterworth filter was applied to the data, and the

accelerations were weighted by vertical factors, w_k, as specified in ISO 2631–1 [50] shown in Fig. 10b. The raw and weighted acceleration time histories of walker (W1) on NB25 and 3SB floors at a walking frequency of $f_w = 2.2$ Hz, are plotted in Fig. 10c and d.
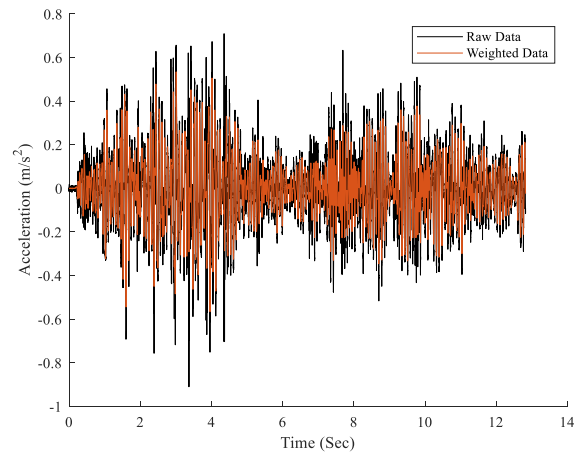
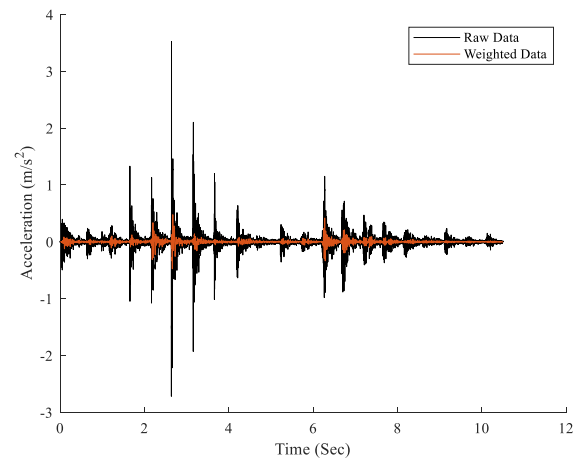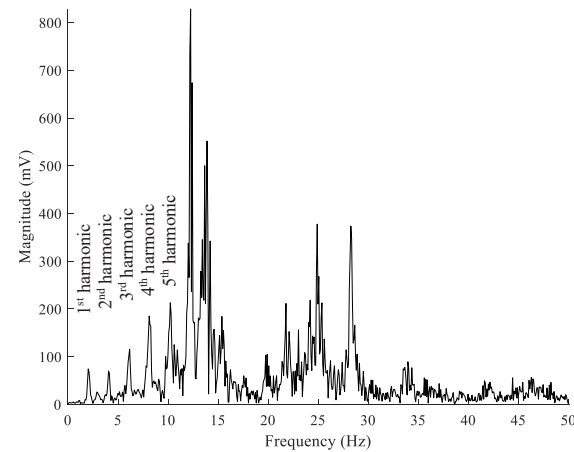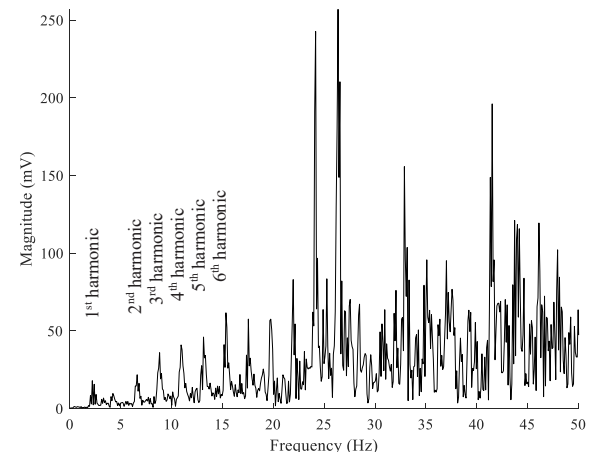As outlined in ISO 10137 [31] the recommended variables to assess
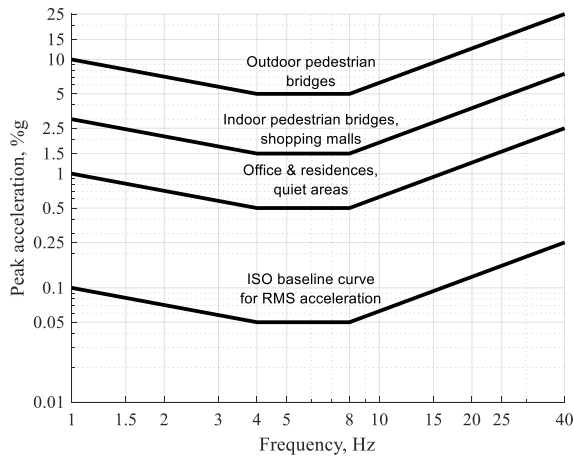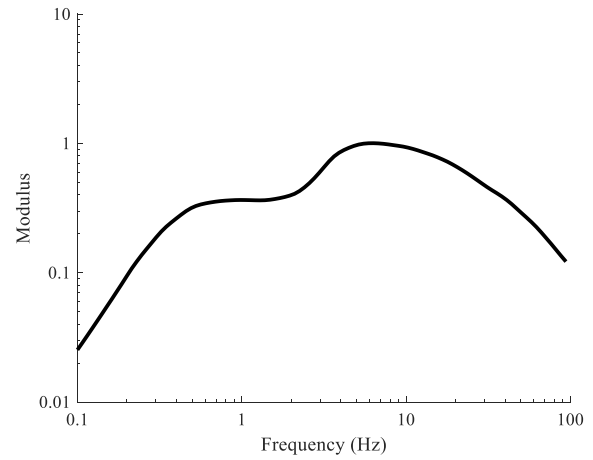
Fig. 10. (a) Base curves for floor vibration design from BS 6472–1 [28] and ISO 10137 [31] showing recommended acceleration tolerance limits for different types of buildings, (b) frequency weighting curve appropriate for vertical vibration BS 6472–1 [28], (c) the raw and weighted acceleration response of W1 walking in NB25 with walking frequency of $f_w = 2.2$ Hz showing a steady-state response, and its frequency domain acceleration response (d) the raw and weighted acceleration response of W1 walking in 3SB with walking frequency of $f_w = 2.2$ Hz showing a transient response, and its frequency domain acceleration response.

vibration serviceability are the root-mean-square acceleration, $a_{w\text{-}rms}$, and the Vibration Dose Value (VDV):

$$a_{w-rms} = \sqrt{\frac{1}{T}\int_0^T a_w(t)^2 dt} \quad VDV = \left\{ \int_0^T [a_w(t)]^4 dt \right\}^{\frac{1}{4}} \quad (6)$$

According to ISO 10137 [31], "*if the ratio of the peak value to the r.m.s. value of the filtered acceleration (taken for the full period of vibration exposure) is greater than 6, the r.m.s. acceptance criteria may not be appropriate and Vibration Dose Values (VDV), which are based upon a* root-mean-quad (r.m.q.) evaluation, can be used". The r.m.s. value of the filtered acceleration, $a_{w\text{-}rms}$, the peak value, $a_{w\text{-}max}$, and the ratio of the latter to the former are represented in Table 6 for all walking scenarios. For ratios smaller than 6, the response factor (RF) is calculated by dividing $a_{w\text{-}rms}$ by 0.005 m/s² (see Fig. 10a). For ratios larger than 6, the VDV is calculated and compared to the threshold VDV of 0.8 (m/s^1.75).

The performance of NB25 and 3SB floors is compared to the acceptable criteria for office floors in ISO 10137 [31] in Table 6. If the requirements are met a (✓) symbol is used. Non-compliant floors are

(a)

(b)
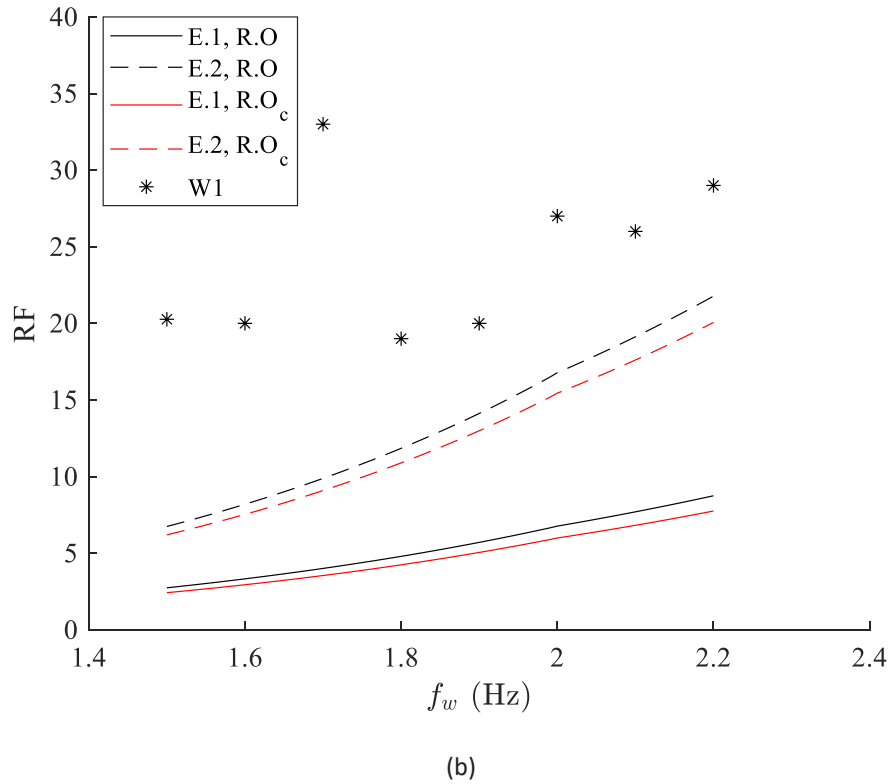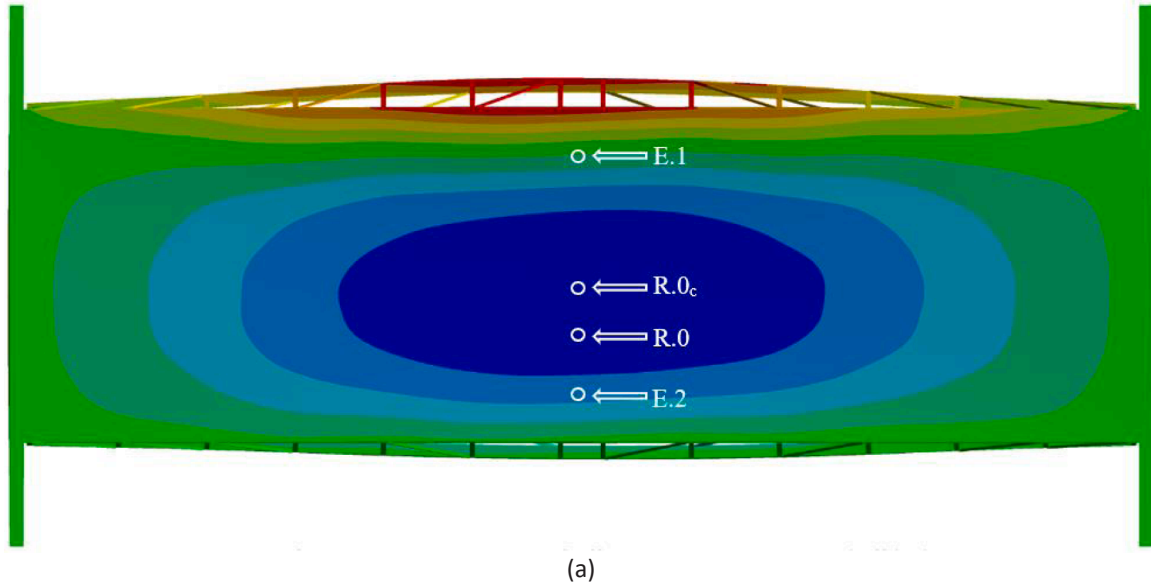
Fig. 11. Response factors from the modal superposition and experiment methods: (a) CCIP-016 [35] prediction for the low-frequency NB25 system over a walking frequency range of 1.5 Hz to 2.2 Hz; (b) comparison of the predicted results with measured data from the walking path shown in Fig. 2 denoted by (*); (c) CCIP-016 [35] prediction for the high-frequency 3SB system over the same walking frequency range; and (d) comparison of the predicted results with measured data from the walking path shown in Fig. 1d denoted by (*).
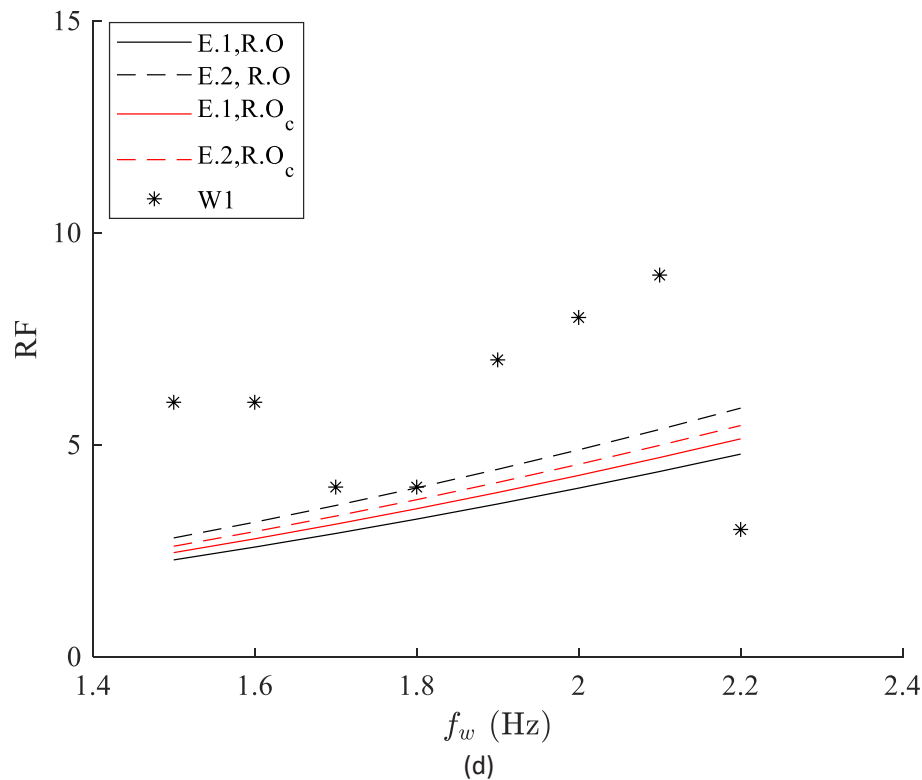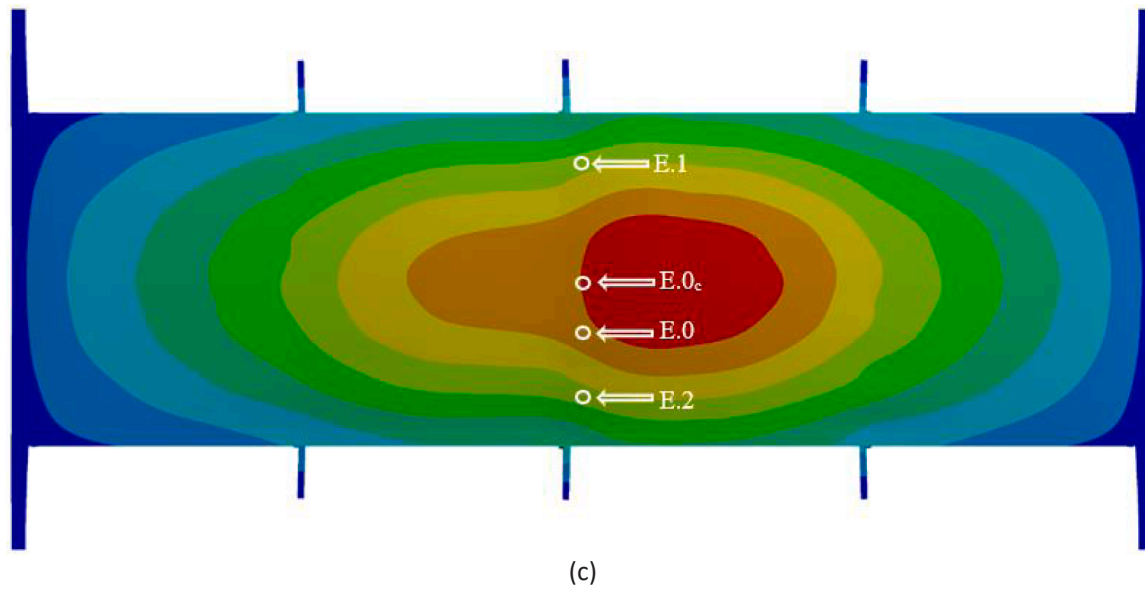
(c)

(d)

Fig. 11. (*continued*).

shown with (×). NB25 is generally unacceptable except in VDV criterion of walker (W2) at f_w of 1.7 Hz and 2.2 Hz. In contrast, 3SB shows acceptable performance across all W1 (with the exception of f_w of 1.6 Hz) and W3 (with the exception of f_w of 1.7 Hz and 1.9 Hz).

A comparison between the RFs calculated using the CCIP-016 [35] methodology and those measured from walking tests with W1 on both the NB25 and 3SB floor systems shows relatively good agreement.

6.2. Participant experiments and surveys

A total of 80 participants were recruited, with 40 assigned to each

floor (NB25 and 3SB) to conduct walking tests and complete perception surveys. Before the test was conducted, each participant was weighed. Unlike the tests presented in Section 6.1, the walkers in this series of tests were not required to walk at a certain frequency. They were asked to walk on the same floor twice, once at their normal walking speed and next at a fast walking speed. Results are shown in Fig. 12 with $a_{w\text{-}rms}$ at measured f_w and are displayed with different colours based on the walkers' weight. Circle symbols denote the NB25 floor and triangle symbols represent 3SB. The acceptance baseline for office floors corresponds to RF of 4 ($a_{w\text{-}rms} = 0.02$ m/s^2) taken from ISO 10137 [31] and is shown on the graphs with solid red line.

Table 6

Responses of the NB25 and 3SB floor systems to walking excitations of walkers W1 (75 kg), W2 (80 kg) and W3 (85 kg) and comparison with acceptance criteria of office floors in ISO 10137 [31].

| f_w (Hz)	$a_{w,\,rms}$ (m/s^2)	$a_{w,max}$ (m/s^2)	$\dfrac{a_{w,max}}{a_{w,rms}}$	RF $\dfrac{a_{w,rms}}{0.005}$	VDV (m/s$^{1.75}$)	RF < 4 ISO 10137 [31]	VDV < 0.8 ISO 10137 [31]
W1 walking on NB25 floor
1.6	0.099	0.572	5.8	20	0.350	×	N/A
1.7	0.165	0.678	4.1	33	0.511	×	N/A
1.8	0.097	0.508	5.2	19	0.318	×	N/A
1.9	0.100	0.520	5.2	20	0.299	×	N/A
2.0	0.134	0.596	4.4	27	0.375	×	N/A
2.1	0.130	0.500	3.8	26	0.344	×	N/A
2.2	0.147	0.535	3.6	29	0.383	×	N/A
W2 walking on NB25 floor
1.6	0.199	0.685	3.4	40	0.555	×	N/A
1.7	0.188	1.617	8.6	38	0.653	N/A	✓
1.8	0.434	3.379	7.8	87	1.646	N/A	×
1.9	0.384	3.095	8.1	77	1.551	N/A	×
2.0	0.409	3.260	8.0	82	1.420	N/A	×
2.1	0.339	1.490	4.4	68	0.909	×	N/A
2.2	0.339	2.158	6.4	68	1.102	N/A	✓
W1 walking on 3SB floor
1.6	0.032	0.414	12.9	6	0.144	✓	N/A
1.7	0.019	0.210	11.1	4	0.078	✓	N/A
1.8	0.022	0.299	13.6	4	0.110	✓	N/A
1.9	0.037	0.335	9.1	7	0.141	N/A	✓
2.0	0.041	0.478	11.7	8	0.180	N/A	✓
2.1	0.047	0.538	11.4	9	0.188	N/A	✓
2.2	0.016	0.199	12.4	3	0.068	✓	N/A
W3 walking on 3SB floor
1.6	0.039	0.599	15.4	8	0.221	N/A	✓
1.7	0.026	0.332	12.8	5	0.127	×	N/A
1.8	0.039	0.425	10.9	8	0.177	N/A	✓
1.9	0.031	0.287	9.3	6	0.105	×	N/A
2.0	0.051	0.710	13.9	10	0.253	N/A	✓
2.1	0.037	0.233	6.3	8	0.125	N/A	✓
2.2	0.051	0.285	5.6	10	0.164	N/A	✓

For normal walking with a measured median walking frequency of 1.64 Hz (vertical dashed line in Fig. 12a), the calculated accelerations for each participant on NB25 demonstrate that the floor falls significantly short of the acceptance criteria. In 3SB at normal walking speeds, about half of the measured responses are within the acceptable acceleration tolerance for an office floor with R= 4. Using a more relaxed response factor of 8, all responses are within the acceptable threshold.

In fast walking speed with a measured median walking frequency of 1.96 Hz (vertical dashed line in Fig. 12b), none of the NB25 responses are in the acceptable range and only a couple of 3SB responses are less than the acceleration threshold for office floors according to ISO 10137 [31].

The human perception survey was based on the questionnaire outlined in ISO/TR 21136 [48]. Participants were asked to rate the floor on a scale from 0 to 100, where 0 represented a completely unacceptable, excessively bouncy floor, and 100 indicated a completely acceptable floor with no vibration issues. For each floor, participants were divided into two groups of 20 individuals. The first group utilised Virtual Reality (VR) during the tests to simulate a work environment rather than a laboratory setting, while the second group performed the tests without VR. Both groups followed identical test procedures. Initially, all participants were seated on the prepared chair and instructed to read a presentation on a laptop or through VR. At the same time, walker W1 (see Section 6.1) walked along the designated path on the floor (see Fig. 2) completing two laps at two different speeds normal walking speed and a fast walking speed simulating a rush to complete a task.

In Fig. 13, the percentage of floor acceptance is plotted on the X-axis against the percentage of participants on the Y-axis. Blue bars represent participants without VR, while red bars correspond to those who used VR. The results for the floor without a strongback (NB25), under normal walking conditions, show that a significant portion of participants without VR (~25 %) rated the floor with an acceptance percentage of approximately 20 %. In contrast, a more even distribution was observed among participants with VR, with peaks around 50 %, 60 %, and 80 %. This suggests that without VR, participants tend to perceive the floor as less acceptable, with a concentration in the lower acceptance range. On the other hand, those using VR appeared to distribute their responses more evenly. During fast walking speed (Fig. 13a), the perception shifted slightly, and 20 % of non-VR participants clustered around a 20 % acceptance rate. However, the VR group demonstrated higher acceptance levels, with peaks around 50 % and 60 %.

The results for the floor with three strongbacks (3SB), under normal walking conditions (Fig. 13b) indicated a noticeable increase in perceived floor vibration. Non-VR participants mostly rated floor acceptance around 40–50 %, with a peak of over 35 % at 50 % floor acceptance. VR participants, on the other hand, distributed their ratings across several acceptance levels, with peaks at 50 %, 70 %, and 90 %. This shift toward higher acceptance ratings may indicate that the floor reinforcement using strongbacks significantly improved participants' comfort and perception of floor vibration during normal walking. In fast walking speed, the trend became even more distinct. Non-VR participants predominantly concentrated their acceptance ratings around 40 %
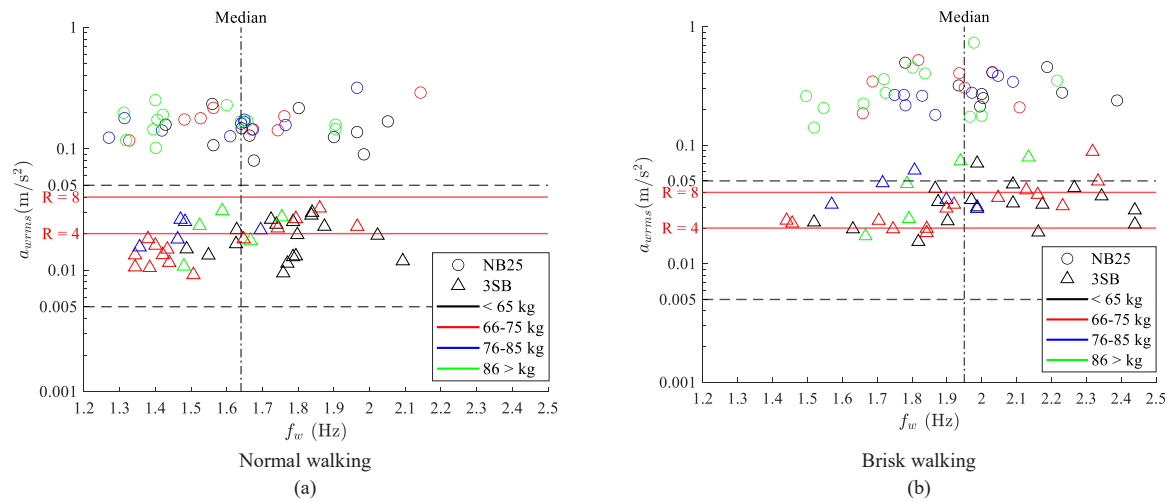
Fig. 12. The r.m.s. value of the filtered acceleration, $a_{w\text{-}rms}$ at different walking frequencies, f_w of all participants showing walker weight distribution, (a) normal walking and (b) brisk walking.
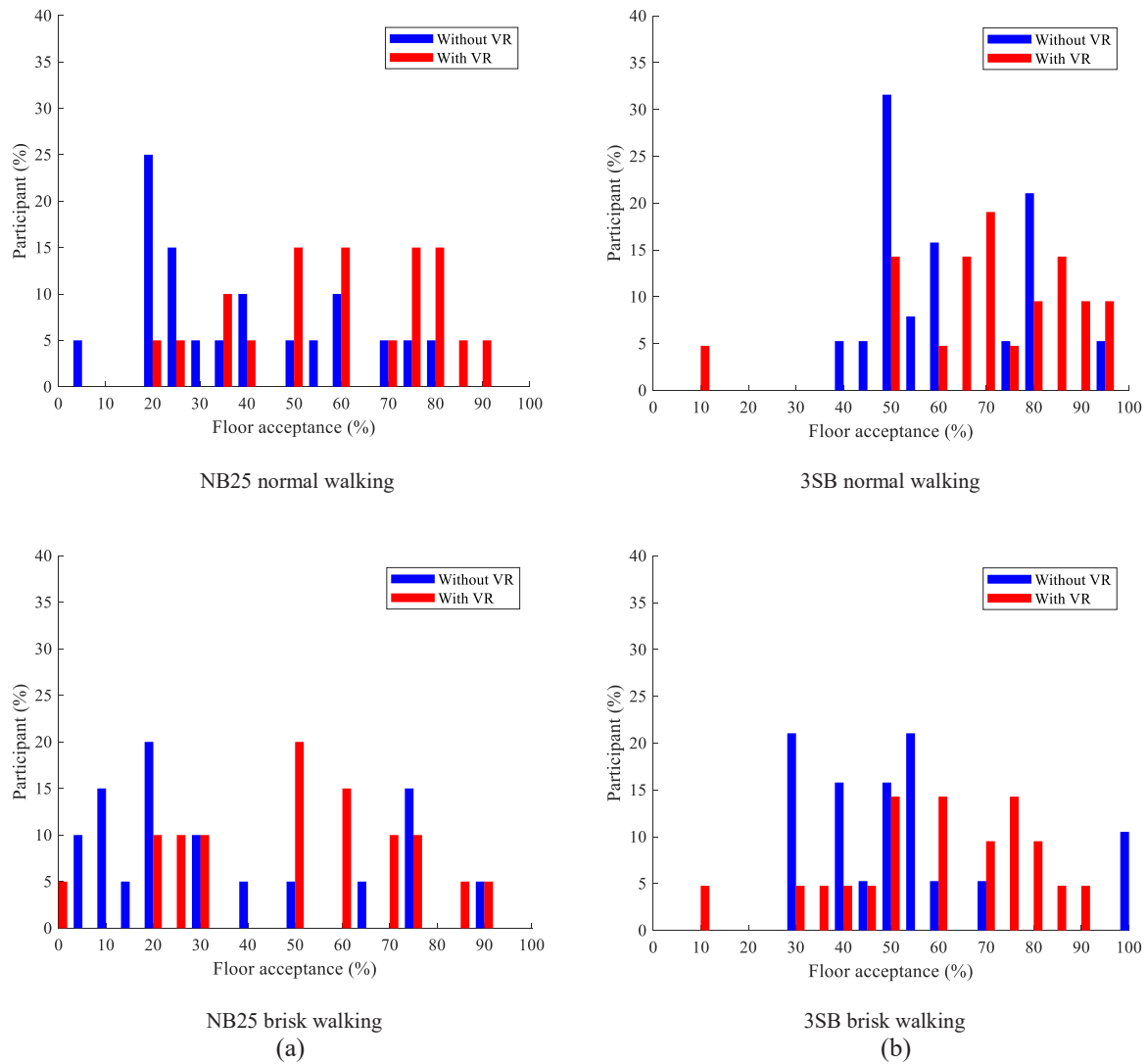
Fig. 13. Perception results of participants' surveys to floor vibration at normal and brisk walking with and without the Virtual Reality tool showing scores from 0 (bouncy floor) to 100 (floor with no adverse comments on vibration).

and 90 %, while VR participants spread their ratings across 50 %, 60 %, and 90 %. This distribution indicates that the strongback reinforcement significantly reduced the adverse effects of brisk walking on perceived vibrations, with participants perceiving the 3SB floor as considerably more acceptable compared to NB25.

7. Conclusions

Experimental and numerical studies were conducted on the performance of an 8-meter-long floor system comprising steel-wood truss joists with a nominal depth of 600 mm, spaced 450 mm center-to-center, and a particleboard slab. The floor's design for vibrations induced by walking excitations was evaluated against international standards and guidelines. The non-strengthened floor met all acceptance criteria outlined in standards/guidelines that rely on static deflection and frequency-deflection methods. However, when subjected to laboratory walking excitations and participant surveys, the floor was largely rated as unacceptable. Additionally, the non-strengthened floor failed to meet the requirements of standards/guidelines based on the modal superposition to calculate vibration response. Based on these findings, it is strongly recommended that comprehensive methods, which involve calculating vibration acceleration from modal analyses, be employed in the design of long-span lightweight floors subjected to walking-induced excitations. It is important to note that most of these methods are calibrated for concrete floors, and discrepancies between their predictions and the measured responses of the floor studied herein highlight the need for further research.

Both experimental methods and numerical analyses demonstrated that incorporating strongbacks in the transverse direction of the floor system effectively reduces its vibration acceleration. No significant change in the measured damping was observed between the non-reinforced floor and the floor with strongbacks. However, the natural frequencies of the floor with strongbacks were significantly increased. Additionally, the torsional mode present in the non-strengthened floor was not observed in the floor with strongbacks.

The study of participants' perception of floor vibration confirmed the suitability of the floor with strongbacks for use in commercial applications. Most notably, the use of virtual reality headsets to isolate participants from the laboratory environment significantly affected their perception of floor suitability.

CRediT authorship contribution statement

Huaizhong Li: Writing – review & editing, Methodology, Investigation. **Guido Carim Junior:** Writing – review & editing, Methodology, Investigation, Conceptualization. **Chandan Kumar:** Writing – review & editing, Supervision, Methodology. **Hassan Karampour:** Writing – review & editing, Validation, Supervision, Software, Resources, Project administration, Methodology, Investigation, Funding acquisition, Data curation, Conceptualization. **Hong Guan:** Writing – review & editing, Supervision, Methodology. **Farid Piran:** Writing – original draft, Validation, Software, Investigation, Formal analysis, Data curation.

Declaration of Competing Interest

The authors declare that they have no known competing financial interests or personal relationships that could have appeared to influence the work reported in this paper.

Acknowledgements

Data availability

Data will be made available on request.

References

[1] Ramage MH, Burridge H, Busse-Wicher M, Fereday G, Reynolds T, Shah DU, et al. The wood from the trees: the use of timber in construction. Renew Sustain Energy Rev 2017;68:333–59.

[2] Liang S, Gu H, Bergman R. Environmental life-cycle assessment and life-cycle cost analysis of a high-rise mass timber building: a case study in Pacific Northwestern United States. Sustainability 2021;13:7831.

[3] Construction; Australian Industry Skills Committee. Australian Industry Skills Committee; 2022.

[4] Mai KQ, Park A, Nguyen KT, Lee K. Full-scale static and dynamic experiments of hybrid CLT–concrete composite floor. Constr Build Mater 2018;170:55–65.

[5] Zhang J, Zhang C, Li Y, Chang W-S, Huang H. Cross-laminated timber (CLT) floor serviceability under multi-person loading: Impact of beam–panel connections. Eng Struct 2023;296:116941.

[6] Hassanieh A, Valipour H, Bradford M. Experimental and numerical investigation of short-term behaviour of CLT-steel composite beams. Eng Struct 2017;144:43–57.

[7] Karampour H, Piran F, Faircloth A, Talebian N, Miller D. Vibration of timber and hybrid floors: a review of methods of measurement, analysis, and design. Buildings 2023;13:1756.

[8] Carradine D. Multi-storey light timber-framed buildings in New Zealand–Engineering design. New Zealand: BRANZ, Judgeford; 2019.

[9] Reiher H, Meister F. The sensitiveness of the human body to vibrations: Wright Field. Air Materiel Command; 1946.

[10] Postlethwaite F. Human susceptibility to vibration. Engineering 1944;157:61–3.

[11] King AJ. Vibration and noise of mechanisms and machines. Engineering 1957:759–66.

[12] Lenzen KH. Vibration of steel joist-concrete slab floors. Eng J 1966;3:133–6.

[13] Wiss JF, Parmelee RA. Human perception of transient vibrations. J Struct Div 1974;100:773–87.

[14] Smith I, Chui YH. Design of lightweight wooden floors to avoid human discomfort. Can J Civ Eng 1988;15:254–62.

[15] Howarth H, Griffin M. Human response to simulated intermittent railway-induced building vibration. J Sound Vib 1988;120:413–20.

[16] Ljunggren F, Wang J, Ågren A. Human vibration perception from single-and dual-frequency components. J Sound Vib 2007;300:13–24.

[17] Ellis B. Serviceability evaluation of floor vibration induced by walking loads. Struct Eng 2001.

[18] Griffin MJ. Handbook of human vibration. Academic press; 2012.

[19] Toratti T, Talja A. Classification of human induced floor vibrations. Build Acoust 2006;13:211–21.

[20] Hamm P, Richter A, Winter S. Floor vibrations–new results. In: Proceedings of eleventh world conference on timber engineerig (WCTE2010), Riva del Garda. 2010.

[21] Brownjohn J, Racic V, Chen J. Universal response spectrum procedure for predicting walking-induced floor vibration. Mech Syst Signal Process 2016;70:741–55.

[22] Brownjohn J, Middleton C. Procedures for vibration serviceability assessment of high-frequency floors. Eng Struct 2008;30:1548–59.

[23] Racic V, Brownjohn JMW. Stochastic model of near-periodic vertical loads due to humans walking. Adv Eng Inform 2011;25:259–75.

[24] Racic V, Pavic A, Brownjohn J. Experimental identification and analytical modelling of human walking forces: Literature review. J Sound Vib 2009;326:1–49.

[25] Chen J, Ding G, Živanović S. Stochastic single footfall trace model for pedestrian walking load. Int J Struct Stab Dyn 2019;19:1950029.

[26] Chang W., Goldsmith T., Harris R. A new design method for timber floors–peak acceleration approach. In: Proceedings of the international network on timber engineering research meeting 2018: Sheffield; 2018.

[27] Structural design actions - Part 0: General principles. Australian Standard AS1170.0; 2002.

[28] British Standards Institution. Guide to evaluation of human exposure to vibration in buildings. London2008.

[29] National Standard of Canadao, CSA 086:19. Engineering design in wood. 2019.

[30] Eurocode 5: Design of timber structures Part 1-1 European Committee for Standardization; 2004.

[31] ISO 10137, International Standards Organisation. Basis for design of structures-serviceability of buildings and walkways against vibrations. Geneva;2007.

[32] Feldmann M, Heinemeyer C, Butz C, Caetano E, Cunha A, Galanti F, et al. Design of floor structures for human induced vibrations. JRC–ECCS joint report; 2009. p. 45.

[33] Murray T, Allen D, Ungar E, Davis DB. Steel design guide series 11: vibrations of steel-framed structural systems due to human activity. Chicago: American Institute of Steel Construction; 2016.

[34] Smith Hicks S, Devine P. Design of floors for vibration: a new approach–revised edition (SCI P354). Ascot: Steel Construction Institute; 2009.

[35] Concrete Centre. A design guide for footfall induced vibration of structures. Camberley, England: The Concrete Society; 2006.

[36] Feldmann M. Human-induced vibration of steel structures (HIVOSS). Luxembourg; 2008.

[37] Australian Standard. 1720.1 Timber structures - part 1: design methods. Sydney; 2010.

[38] Australian Standard. Steel structures. AS 4100. Sydney;2020.

[39] ASTM International. Standard test methods for evaluating properties of wood-base fiber and particle panel materials, ASTM D1037–12 United States;2012.

[40] Labonnote N, Rønnquist A, Malo KA. Prediction of material damping in timber floors, and subsequent evaluation of structural damping. Mater Struct 2015;48: 1965–75.

[41] ANSYS I. ANSYS mechanical 2021/R2. Canonsburg, PA;.2021.

[42] DeSalvo GJ, Swanson JA. ANSYS engineering analysis system: user's manual. Houston: Swanson Analysis Systems; 2022.

[43] Stamatopoulos H, Malo KA. Withdrawal capacity of threaded rods embedded in timber elements. Constr Build Mater 2015;94:387–97.

[44] Masaeli M, Karampour H, Gilbert BP, Guan H, Behnia A, Talebian N. Numerical evaluation of failure mechanisms and retrofitting of connections in mass timber buildings. KSCE J Civ Eng 2023;27:3019–35.

[45] Timber structures-Test methods, Floor vibration performance. Geneva: ISO 18324; 2016.

[46] Australian Standard. 1170.1 Structureal design action - Part 1: permanent, imposed and other actions. Sydney;2002.

[47] Building Code. International Residential Code. International Energy. 2018.

[48] ISO/TR 21136: Timber structures — Vibration performance criteria for timber floors. Geneva: ISO/TR 21136; 2017.

[49] Feldmann M, Heinemeyer C, Lukic M. Design of footbridges. guideline. Human induced vibrations of steel structure (Hivoss) 2008. Hivoss-RFS2-CT-2007-00033.

[50] AS 2670.1 - ISO 2631-1. Evaluation of human exposure to whole-body vibration part 1: general requirements. Sydney, Australia: ISO; 2001.